

UC Santa Cruz

UC Santa Cruz Electronic Theses and Dissertations

Title

The role of Förster Resonance Energy Transfer in luminescent solar concentrator efficiency and color tunability

Permalink

<https://escholarship.org/uc/item/0q91q6vj>

Author

Balaban, Benjamin

Publication Date

2013

Peer reviewed|Thesis/dissertation

UNIVERSITY OF CALIFORNIA
SANTA CRUZ

**THE ROLE OF FÖRSTER RESONANCE ENERGY TRANSFER IN
LUMINESCENT SOLAR CONCENTRATOR EFFICIENCY AND COLOR
TUNABILITY**

A dissertation submitted in partial satisfaction

of the requirements for the degree of

DOCTOR OF PHILOSOPHY

in

PHYSICS

by

Benjamin L. Balaban

September 2013

The Dissertation of Benjamin L. Balaban
is approved:

Dr. Sue A. Carter, Chair

Dr. Glenn B. Alers

Dr. Frank Bridges

Tyrus Miller
Vice Provost and Dean of Graduate Studies

Table of Contents

1. Introduction

1.1 Planar luminescent solar concentrator devices	1
1.2 Fluorescent species used in LSC devices, previous considerations	9
1.3 1.3 Nonradiative energy transfer - mechanism and historical context	13

2. Sample preparation

2.1 Doctor-bladed sample preparation: determining FRET concentration regime	26
2.2 LSC device sample preparation	27

3. Experiment and discussion

3.1 Establishing FRET dominance as a function of dye:host concentration	30
3.2 FRET, AM1.5 Absorption, Film Self Absorption	46
3.3 The effect of FRET on waveguide transport losses	50

4. Perceived film color

4.1 The role of FRET, fluorescence spectrum on film color.....	63
4.2 LSC color calculation from a subtractive CMY color model	66

5. Conclusions

74

References

76

List of Figures

1.1.1 Sample LSC device layout showing side mounted PV modules. Figure depicts an LSC layer (b) optically coupled to a non-fluorescent waveguide (a). Incident light is absorbed by the dye molecules (d) and re-emitted isotropically (g). About 25% is not internally reflected and lost through the escape cone (f). The remainder is trapped in the waveguide (e) and collected at properly positioned PV cells (c). Reproduced from [1].	2
1.1.2 Early LSC concept introduced by Keil. Figure shows a PV module (used as a photodetector) coupled into a waveguide made from a fluorescent plexiglass material. Reproduced from [2]	2
1.1.3 Two dimensional cross section of the isotropic emission sphere of a fluorophore in an LSC. ~75% of the total emission sphere surface area (solid angle) will be trapped within the waveguide from total internal reflection.	5
1.2.1 Chemical structures of BASF Lumogen F Red 305, a Perylene Diimide, and Exciton DCM, a merocyanine.	9
1.2.2 Emission spectra of Exciton DCM under 460 nm excitation in Methanol (at 10^{-6} M) and in PMMA. Peak optical density is <0.1 in both cases to minimize self-absorption effects. DCM is highly subject to solvation effects and, unlike LR305, its spectroscopic properties vary widely as a function of concentration and host	11
1.2.3 Depiction of -R position substituents shown to increase perylene diimide solubility in the work of Seybold and Wagenblast. Reproduced from [5].	12
1.3.1 Semilog plot depicting fluorescence anisotropy and intensity of fluorescein in glycerine as a function of concentration. Depolarization of fluorescence is seen to happen in a much lower concentration regime than explainable by self-absorption of fluorescence. Reproduced from [22]	19
1.3.2 Behavior of the electric field vector in the near-field region of a Hertzian dipole. Field patterns are distinct from those in the radiation zone. Reproduced from [62].	25
2.1.1 0.75% LR305 film in PMMA, 0.5% DCM film in PMMA, 0.75% LR305/0.5% DCM blend (left to right, percentages by weight).	27
2.2.1 Sample LSC device construction (not drawn to scale). An absorbing LSC layer (polymer doped with dyes) is optically sandwiched between two 3 mm glass plates. The polymer is index matched to the glass.	28
2.2.2 "Low" (left) and "high" (right) density LSC samples, with coupled PV modules and inactive edges coated with absorbing ink. The absorbing layer of the low density	

sample is 0.05% dye:polymer (by weight) and 600 microns thick. High density sample absorbing layer is 0.25% dye:polymer and 120 microns thick.	30
3.1.1 Normalized absorption and emission spectra of LR305 and DCM dyes in PMMA.	31
3.1.2 Emission spectra of spin-cast, low optical density LR305 films in PMMA. No change in emission is observed between 440 nm and 590 nm excitation.....	32
3.1.3 Comparison of 0.5% donor (DCM), and 0.75% acceptor (LR305) wavelength dependent optical density (top). Blended film absorbance of same concentrations (1.25% total dye) is compared with a sum of the optical densities at each wavelength (bottom).	34
3.1.4 Comparison of the emission spectra of stacked and blended LR305/DCM 0.75%/0.5% PMMA films when excited with 460 nm light. The "blended single film" is a single layer containing both 0.75% LR305:PMMA and 0.5% DCM:PMMA. "Stacked" films (illustrated above) are comprised of single-dye films (0.75% LR305:PMMA on top, 0.5% DCM:PMMA on the bottom) physically stacked on top of one another, with the LR305 "acceptor" film closer to the detection and excitation source. As such, any DCM emission would necessarily pass through the full LR305 optical density. Despite this, the stacked films show strong DCM fluorescence while the blend shows almost none.	35
3.1.5 Normalized emission spectra of 0.625% DCM:PMMA films with varying levels of LR305 dye added. 460 nm excitation used in all cases. DCM emission is seen to be quenched with increasing LR305, however optical density of added LR305 is much lower than necessary to explain DCM fluorescence quenching.	37
3.1.6 Absorption spectra of LR305 films. Compare with figure 3.1.5. A 5 micron thick 0.5% LR305 film has approximately 17% absorption at 555 nm, but mixing 0.5% LR305 into a 5 micron thick DCM film quenches over 85% of its 555 nm fluorescence (as seen in figure 3.1.5).	37
3.1.7 604 nm emission intensity as excitation wavelength is swept across the absorption range of LR305 and DCM. The blended film shows enhanced LR305 emission response in the range of DCM's absorption. Intensities given in relative but arbitrary units (RU).	39
3.3.8 Emission spectra of 0.75% LR305 films under 460 nm excitation. Absorption spectra of 0.75% LR305 and 0.0625% DCM films are also shown. The addition of 0.0625% DCM increases the 460nm absorption of the LR305 film by almost exactly 50%. A corresponding enhancement in LR305 emission is also seen (by integrated spectrum). 0.75% LR305 5 micron films absorb <30% at their peak (and considering	

entire optical density of the film), and DCM has a quantum yield of 76% in PMMA. Emission enhancement therefore exceeds that possible from radiative transfer. Intensities given in relative but arbitrary units..	39
3.1.9 Sample non-normalized emission profiles of 1:2 weight ratio LR305/DCM films under 460 nm excitation. DCM emissions is quenched as concentration rises. Intensities given in relative but arbitrary units (RU).	42
3.1.10 Sample non-normalized emission profiles of 3:2 weight ratio LR305/DCM films under 460 nm excitation. The same effect is again seen.	42
3.1.11 Recovery of approximate {concentration} ^{-1/3} intermolecular distance from least squares fit of leading coefficient to calculated D-A pair distances.	45
3.1.12 Plot of calculated donor-acceptor pair distance as a function of acceptor concentration with donors added in different ratios. Given the R-6 transfer probability dependence, acceptor interaction with a "nearest" donor is substantially more likely than interaction with more distant donors. Similarly, donor-donor non-radiative homotransfer has a substantially lower probability in the concentration regime surrounding the donor-acceptor critical distance.	45
3.2.1 Increases in the 575 nm (peak) optical density of L305 provide progressively less benefit to AM1.5 absorption, at the expense of greatly increased self-absorption of emitted light. Transmission at given peak optical density is plotted against LR305's own emission to highlight the increase in self-absorption in high optical density LR305 films.	48
3.2.2 Percentage of AM1.5 Intensity spectrum absorbed by an LR305 film as a function of its peak optical density. Higher optical density films continue to increase self absorption with progressively less solar photon flux absorption.	48
3.2.3 Comparison of the peak fluorescence intensity of DCM blended and LR305 only films in different ratios as the concentration is varied. Lower acceptor:donor ratios allow for less self absorption of emitted light, reducing the inner filter effect and facilitating brighter surface fluorescence.	50
3.3.1 Excitation wavelength dependent quantum yield measurements of the short and long wavelength dyes in EVA, as measured by Hamamatsu PL QY spectrometer...	52
3.3.2 Emission and absorbance spectra of the short and long wavelength dyes used in this section. Emission spectra taken with excitation at respective peak absorbance wavelengths.	53
3.3.3 Calculated FRET efficiency as a function of D-A pair separation for short and long wavelength dyes used in this experiment.	54

3.3.4 Experimental determination of LSC sample edge emission under 405 nm excitation.	55
3.3.5 Comparison of the "low" and "high" concentration LSC sample edge emission with the thin-film emission from an "acceptor" (long wavelength dye) only film. ...	55
3.3.6 EQE measurement of a cSi cell used in the experiment. Response is seen to be even across the range of the emission spectrum detected at the LSC edge.	57
3.3.7 Sample LSC device with intensity calibrated excitation visible in the device's center.	58
3.3.8 Schematic showing how R_0 (the distance from the point of excitation to the center of the center cell) is defined to calculate the geometric normalization factor G_{nc} . LSC is viewed from above in this figure.	59
3.3.9 Average "adjusted" EQE (averaging the wavelength dependent adjusted EQE over the relevant range).	60
3.3.10 Comparison of transport efficiency between the "low" and "high" density LSC samples as a function of excitation wavelength. Absorbance spectra of short and long wavelength dyes are shown for comparison. Note that the adjusted EQE normalizes against absorption of each film.	62
4.1.1 Comparison of transmitted light both with (thin film measurement system) and without (dual-monochrometer UV-Vis spectrometer) fluorescence intensity	63
4.1.2 Various color possibilities are plotted on a CIE 1931 xy chromaticity diagram. Data are taken from samples measured with the thin film measurement system described in section 2.1. CIE 1931 xy chromaticity may be derived from CIE XYZ colorspace values from a suitable transformation.	65
4.2.1 Figure 4.2.1: A normalized sample D65 spectrum.	67
4.2.2 CIE XYZ color matching functions used to determine CIE XYZ values. Color matching functions are determined largely from the spectral response of human color receptors.	70
4.2.3 Overlay of primary subtractive colors: cyan, magenta, and yellow absorbers may be combined to cover a large portion of the visible spectrum.	71
4.2.4 Absorbance spectra of approximate "primary color" absorbers. Note that the absorption spectra are coded according to how they appear when their absorption is subtracted from a white light source - while the "cyan" absorber has an absorption peak in the red, it has higher transmission in the blue, thus its perceived color, one weighted against the spectral response of human color receptors (see figure 4.2.2).	72

Abstract

The role of Förster Resonance Energy Transfer in luminescent solar concentrator efficiency and color tunability

by

Benjamin L. Balaban

Förster-type resonance energy transfer (FRET) is demonstrated in a luminescent solar concentrator (LSC) material containing two air-stable, high quantum yield laser dyes in a PMMA matrix. The concentration regime surrounding the Förster critical distance is determined for the system. Two-dye LSC films employing FRET are shown to increase the absorption of air mass 1.5 solar irradiance without affecting the self absorption properties of the film. The impact of nonradiative transfer efficiency on LSC performance is experimentally demonstrated and evidence is presented suggesting higher concentration two-dye films have reduced waveguide transport losses under excitation of the shorter wavelength dye when compared to less concentrated films of the same optical density. The impact of FRET efficiency and thus LSC film fluorescence spectra on LSC color determination is investigated and shown to be minimal. LSC color determination is shown to be accurate through the use of standard subtractive color schemes that consider only film absorption, and wide color tunability is shown to be achievable through the use of a subtractive color model, with as few as three appropriately absorbing dyes.

Chapter 1

Introduction

1.1 Planar luminescent solar concentrator devices

Luminescent solar concentrators (LSCs) offer low cost improvements to building-integrated photovoltaics. An LSC generally consists of an optically transparent material with an index of refraction similar to that of glass doped or coated with a fluorescent downconversion material which absorbs solar radiation and isotropically reemits it at longer wavelengths with a high quantum yield. Thus, a certain percentage of the reemitted light is subject to total internal reflection (about 75%, for a material with an index of refraction of 1.5 - see equation 1.1.3) and trapped in the waveguide. The trapped photons are then absorbed by strips of active PV material optically coupled into the waveguide in a variety of potential geometries. The concept can be illustrated with the examples from [1] shown in figure 1.1.1.

The history of the LSC can be traced back at least 60 years, stemming from the development of scintillation detectors. The 1969 experimental results of Keil [2] drew on the ideas of Shurcliff [3] and Garwin [4] from the previous two decades to experimentally quantify the hypothesized geometric gains of a scintillation detector which closely resembles a planar LSC (figure 1.1.2).

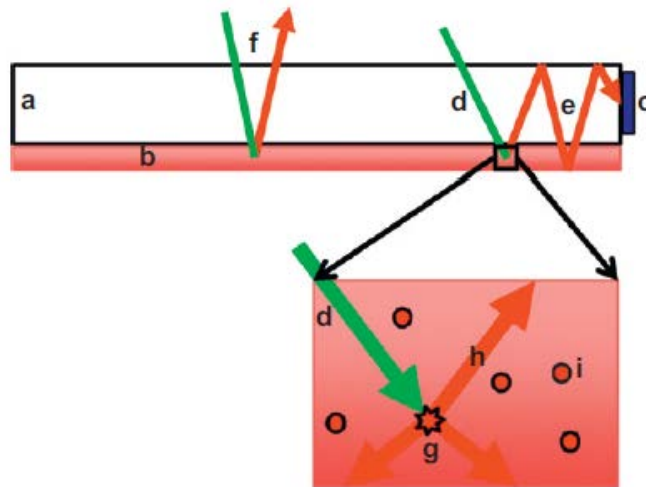


Figure 1.1.1: Sample LSC device layout showing side mounted PV modules. Figure depicts an LSC layer (b) optically coupled to a non-fluorescent waveguide (a). Incident light is absorbed by the dye molecules (d) and re-emitted isotropically (g). About 25% is not internally reflected and lost through the escape cone (f). The remainder is trapped in the waveguide (e) and collected at properly positioned PV cells (c). Reproduced from [1].

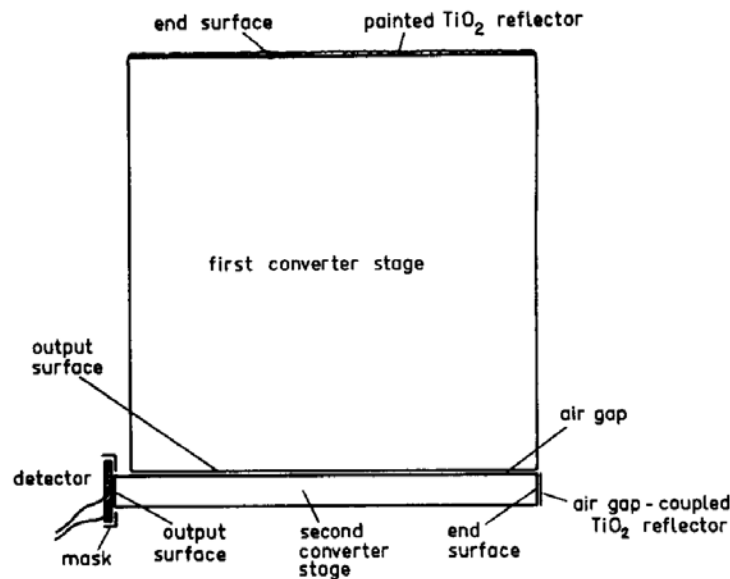


Figure 1.1.2: Early LSC concept introduced by Keil. Figure shows a PV module (used as a photodetector) coupled into a waveguide made from a fluorescent plexiglass material. Reproduced from [2].

While power generation was not mentioned as an explicit goal of [2], a Siemens silicon solar cell was used as a photodetector, with commercial fluorescent plexiglass constituting the waveguide material. The author even went so far as to discuss the enhancement to the quantum efficiency of the solar cell stemming from the downconversion of UV excitation from a mercury discharge lamp. Although this work is noted for its pioneering consideration of the "fluorescent solar collector" concept in the publications of Seybold and Wagenblast [5], who would later develop highly soluble, relatively stable perylene 'dyestuffs' specifically for solar concentrator applications, the 1976 publication of Weber and Lambe [6] is variously cited as the first published LSC concept, while several review articles [7],[8] note from [9] that a 1973 NSF proposal by R.M. Lerner is considered to be its unpublished introduction.

In the proposal of the LSC concept by Weber and Lambe [6], the overall efficiency of an LSC device was defined as the product of three efficiencies:

$$E = \eta Q_A Q_C \quad (1.1.1)$$

η gave the fluorescence quantum yield of the material with Q_A denoting the absorption of solar photon flux, defined by:

$$Q_A = \frac{\int_0^{\lambda_c} N(\lambda) [1 - e^{-\alpha(\lambda)d}] d\lambda}{\int_0^{\lambda_c} N(\lambda) d\lambda} \quad (1.1.2)$$

where the total number of photons absorbed are divided by the total amount incident:

$N(\lambda)$ represents the spectrum of the incident solar radiation, taken in [6] to be an ideal

5500-K blackbody source, but represented by measured AM1.5 data published by NREL in section 3.2 of this work. $\alpha(\lambda)$ is the wavelength dependent Napierian extinction coefficient of the LSC material and d its thickness, such that $1 - e^{-\alpha(\lambda)d}$ is absorption at a wavelength in the interval $\lambda+d\lambda$. In [6], the integral is performed to the cutoff wavelength, λ_c , of the photovoltaic material used (although in this work integration over the full AM1.5 spectrum is considered). Finally, Q_C was defined as the "collection efficiency," which takes into account geometric losses both from the initial reemission and subsequent re-absorption and emission events, as well as losses from reflection when light travels from a relatively low refractive index waveguide into a semiconductor photovoltaic material. In practice, Q_C is fundamentally limited by the "escape cone" of the LSC waveguide, which is determined by the critical angle of the host material-air interface, calculable from the index of refraction of the host material. The probability that an isotropic dye emission event will be trapped in the waveguide, is determined by subtracting the solid angle subtended by the escape cone from the total surface area of uniform spherical emission such that the efficiency of total internal reflection is given by:

$$I_{escape} = \frac{2}{4\pi} \iint_S \sin \theta d\theta d\phi = \int_0^{\theta_c} \sin \theta d\theta = 1 - \frac{\sqrt{n^2 - 1}}{n} \Rightarrow TIR_{Eff} = \frac{\sqrt{n^2 - 1}}{n} \quad (1.1.3)$$

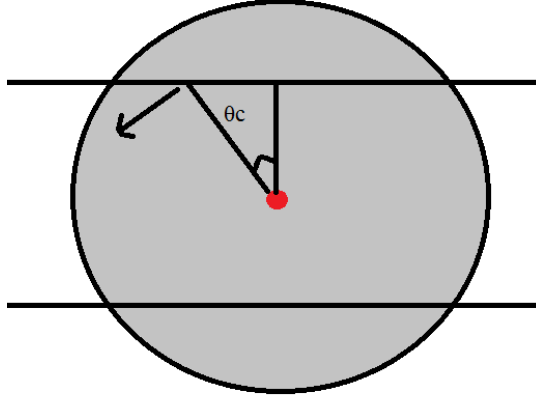


Figure 1.1.3: Two dimensional cross section of the isotropic emission sphere of a fluorophore in an LSC. ~75% of the total emission sphere surface area (solid angle) will be trapped within the waveguide from total internal reflection.

where n is the index of refraction of the host medium, and the critical angle, θ_c , is

given by $\theta_c = \sin^{-1} \frac{1}{n}$ from Snell's law.

As discussed in chapter 3 of this work, maximizing nonradiative energy transfer between multiple absorbers in an LSC will allow the increase of Q_A without the associated transport losses to Q_C , although it has also been shown [10] that the low quantum yield of a donor fluorophore may also be enhanced in certain circumstances through nonradiative transfer of its exciton to a higher quantum yield acceptor. This phenomenon, however, is of limited use to current LSC applications: as noted in [11], fluorophore quantum yield is generally seen to decrease as a function of increasing spectral emission region wavelength - such that downconversion through nonradiative energy transfer (the mechanics of which are discussed in section 1.3) would generally involve an acceptor of similar or lesser quantum yield. Thus,

given approximately equal quantum yields of all the dyes, the main benefit should come from reducing the number of re-emission and absorption events and thus total escape cone and quantum yield losses.

Initial interest in solar concentrator devices was sparked in the mid to late 1970s [7]. Oil supply shock coupled with an inflation adjusted cost per watt of PV modules around two orders of magnitude higher than today [12] motivated a search for cost effective concentration mechanisms allowing for maximal PV power output from a minimal amount of area. The considerably lower cost per watt of solar in today's market has led to a re-evaluation of the economics of LSC schemes, with recent potential application focused on cells which receive both direct and waveguide illumination and close attention paid to installed cost per watt [1]. In these types of layouts, self absorption of the LSC will determine the optimal arrangement of face mounted photovoltaic cells [1],[13] and building integrated PV will generally require higher transparency and thus push low concentration limits for aesthetic purposes.

Although progress has been made within the past several decades in the stability of organic dyes used in LSCs such as Rhodamine [14], and Perylene dyes with the work of Seybold and Wagenblast at BASF [5], LSCs have been inherently limited in power efficiency by low absorption of the solar spectrum, self-absorption of the emitted light, and waveguide losses. While attempts have been made to improve efficiency and maintain stability by increasing absorption using quantum dots [15],[16], broadening absorption and tuning emission through dye interaction with the host environment [17], or using dipole alignment to reduce escape cone

losses [18],[19], the largest single loss is often the narrow absorption spectra of many proposed LSC materials [13]. Early study of planar concentration devices quickly defined the relevant geometric considerations and quantified the related losses [6]. Shortly thereafter, the idea of constructing multiple-dye LSC films to increase absorption was studied [20]. While the prospect of exciton transfer through resonance between a donor's fluorescence transition dipole and a corresponding transition of an acceptor (Förster-type nonradiative transfer) was immediately considered, it was estimated to play a small role in the experiments carried out by Swartz et al. [20] as the concentrations of dye used were too low. More recent undertakings have studied overall efficiency in an LSC system where FRET was shown to be the dominant transfer mechanism between three chromophores [21], but no discussion was made of the concentration regime at which FRET began to occur in a PMMA matrix.

Förster Resonance Energy Transfer, often referred to as FRET, is a type of nonradiative energy transfer between molecules. The process is named for Theodore Förster, who in the years following the second world war published a series of papers culminating in one of his most famous works [22] which drew from the foundations of quantum mechanical theory a framework capable of explaining spectroscopic phenomena involving fluorescing molecules in viscous solutions and solid matrices. The history surrounding his work is discussed in section 1.3. The often cited result of his famous formula (equation 1.3.2), however, is a well known relationship which, in certain circumstances, can provide an accurate estimate of the distance between fluorescing molecules based on fluorescence intensity or lifetime measurements. In

practice, however, average donor-acceptor pair distance calculation can be less straightforward than a cursory glance at Förster's well known relations suggests. While the relations are generally used to estimate Förster-type transfer efficiency between fluorophores in fixed positions, such as those bound to specific sites on proteins and used for biolabeling [23], in a polymer matrix a distribution of distances must be considered. Further complicating matters is that a polymer LSC host matrix does not guarantee a uniform distribution of dopants, leading to quenching-pair distance relations which are nontrivial to calculate numerically [24]. Specifically, mathematical models relating dopant distributions to FRET quenching in a two-dye system have been proposed as a means of gaining insight into the morphology of porous materials such as polymers, among other things [25]. Such models require time-resolved fluorescence measurements and, in the case of [25], neglect homotransfer and consider only transfers between isolated donor-acceptor pairs - a very low concentration situation that is of limited utility when considering solar concentrator applications.

The self absorption characteristics of planar LSC films have similarly been well studied for DCM and Lumogen F dyes specifically [13],[26], [27]. For any given LSC geometry, there is a tradeoff between increasing AM1.5 photon capture and the associated geometric losses from self absorption and lowered quantum yield due to possible aggregate formation and other quenching effects. Thus, for LSC devices containing multiple fluorescent species, a knowledge of the concentration regimes at

which FRET begins to occur is important to consider when optimizing dye concentrations against geometric gains.

In light of these considerations, it is useful to quantify concentration dependent FRET experimentally in a PMMA-host planar LSC setup. It is in this context that the findings of this work are presented with a spectroscopic study of two dye systems, as well as to investigate what experimentally measurable benefits can be seen in changes to waveguide transport losses.

1.2 Fluorescent species used in LSC devices, previous considerations

Both BASF LR305 and DCM have a published history of use as LSC materials. The chemical structures of the two dyes are shown in figure 1.2.1.

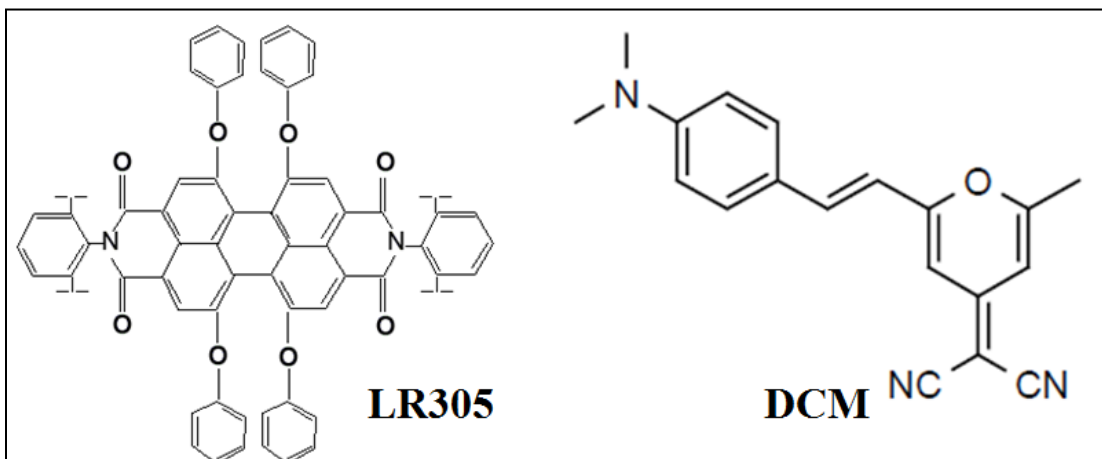


Figure 1.2.1: Chemical structures of BASF Lumogen F Red 305, a Perylene Diimide, and Exicton DCM, a merocyanine.

4-dicyano-methylene-2-methyl-6-p-dimethyl amino-styryl-4H-pyran (DCM) has been previously studied for use as an LSC dye [26]. Two years prior, a comprehensive

experimental LSC study conducted by Batchelder et. al. [28] had shown DCM to be a promising candidate for LSC use because of its broad absorption band and large Stokes shift. As noted in [28], however, DCM was found to have a markedly smaller Stokes' shift in PMMA when compared with its emission in a polar solvent. Like other merocyanines, DCM is prone to solvatochromatic effects. In early studies of merocyanine dyes similar to DCM, Brooker [29] describes how a merocyanine dye "may be regarded as a resonance hybrid between an uncharged and polar structure," and noted that solvent polarity often had a notable effect on the dyes' spectroscopic properties through stabilization of ground and excited states. The effect has been discussed as it specifically pertains to DCM as well - its emission peak has been shown to redshift from approximately 550 nm to 600 nm or more as established by the polarity of its host environment [30]. Such shifts have also been observed in the course of the work presented here, as can be seen in figure 1.2.2, which plots the relative fluorescence peaks of DCM taken both in PMMA films and 10^{-6} M methanol solutions, each under 460 nm excitation. The 554 nm peak emission observed in film is characteristic of DCM's behavior in low-polarity host environments which has been shown to have a quantum yield of 80% in an aqueous solution [20],[31] and 76% in PMMA [31].

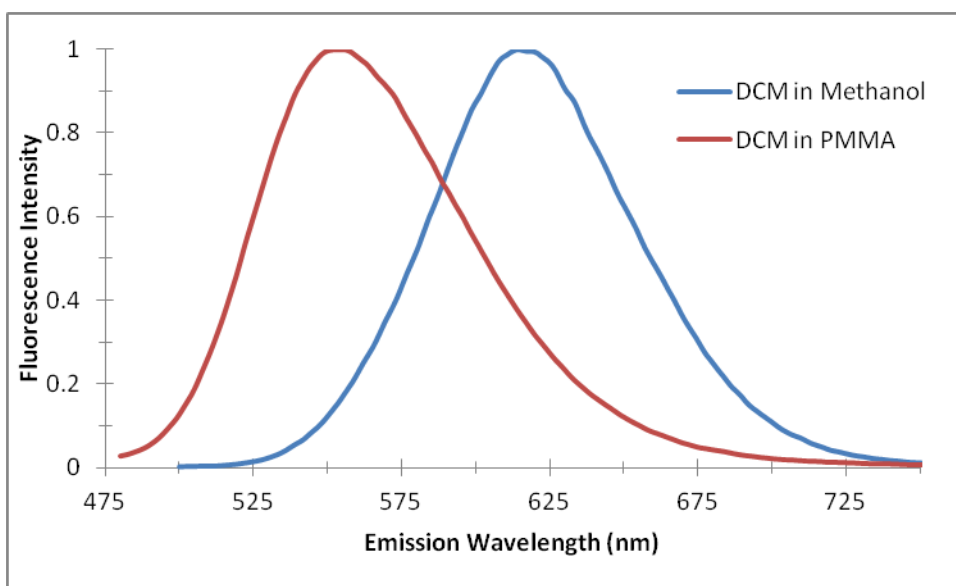


Figure 1.2.2: Emission spectra of Exciton DCM under 460 nm excitation in Methanol (at 10^{-6} M) and in PMMA. Peak optical density is <0.1 in both cases to minimize self-absorption effects. DCM is highly subject to solvation effects and, unlike LR305, its spectroscopic properties vary widely as a function of concentration and host.

BASF Lumogen Red 305, a perylene diimide, is part of a class of structures that have been used in industrial pigments for at least a century [32]. In [5], the effects of various substituents in the "cap" and "bay" positions of the perylene aromatic scaffold on solubility and photostability are studied. As noted in [5], perylene compounds of "type 3" (figure 1.2.3) were in the past shown to have relatively good photostability but limited solubility. Seybold notes that the substitution of ortho-alkyl aromatics into the R position markedly improves solubility, while substitution of phenoxy groups into the bay positions furthers this, without loss to quantum yield or stability, while also providing a redshift for both the absorption and emission bands. The stability, good solubility, and multiple absorption peaks of such types of dyes, and specifically LR305, has led to their frequent

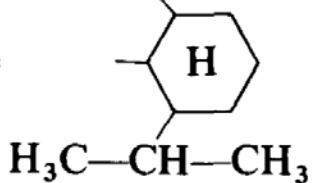
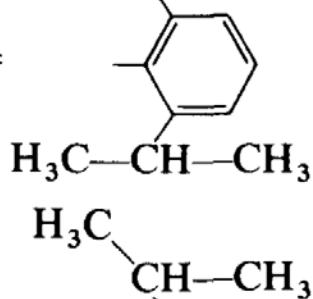
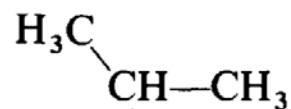
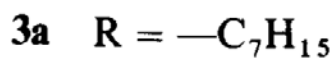
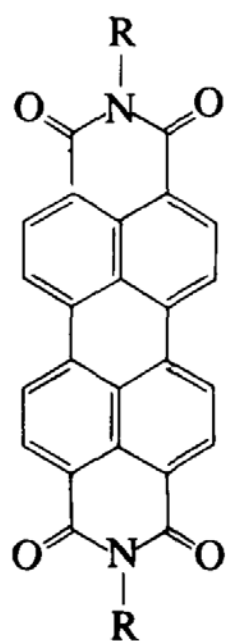


Figure 1.2.3: Depiction of -R position substituents shown to increase perylene diimide solubility in the work of Seybold and Wagenblast. Reproduced from [5].

consideration for LSC applications. The dyes were chosen for use in this work in the context of their use in previous literature, and complimentary spectroscopic properties for the purpose of demonstrating FRET in a solid host matrix. In order to understand the applicability and limitations of Förster's work, it is useful to consider the mechanism and history surrounding his 1948 publication [22].

1.3 Nonradiative energy transfer - mechanism and historical context

Observation of and theoretical explanations for nonradiative energy transfer between multiple fluorescent species predate Förster's famous 1948 publication [22] by several decades. Förster's own historical review of the field [33] cites the first published observation of nonradiative energy transfer between fluorescing species as the work of Cario and Franck [34]. In their work, a diffuse mixture of mercury and thallium gases was excited at the 254 nm mercury resonance line. Such excitation showed 535 nm thallium emission as well. It had already been shown [35] that the thallium vapor would not be excited by either the original excitation or subsequent reemission by mercury, and it was observed that a nonradiative type of energy transfer must be taking place. The process was said to be the "sensitization" of thallium emission to the mercury resonance line, a process Förster noted as analogous to the "donor" and "acceptor" terminology. The proposed mechanism in their paper, however, was collisional: their work extended to interatomic interaction the idea proposed by Klein and Rosseland [36] in which an atom or molecule in an excited state could be de-excited through an interaction with a slow-moving electron. In such a process, the energy difference between the excited and stationary state of the atom is converted to the electron's kinetic energy through an inelastic collision, dubbed "Stöße zweiter Art" (collisions of the second kind) by the authors. The Klein-Rosseland paper was itself postulated to be the reverse process of the 1914 Franck-Hertz experiment [37], in which collisions of electrons with mercury gas atoms were shown to be elastic until the electrons were driven at a potential such that their kinetic energy exceeded that

required to excite mercury atoms from the ground state. Here, inelastic collisions between electrons and mercury atoms were shown to produce mercury emission, with a corresponding drop in electron energy measurable through drops in current through a tube filled with diffuse mercury gas. The drops occurred only at specific applied potentials such that the electron kinetic energy corresponded to integer multiples of quantized transitions from the ground state of mercury. Thus, Franck and Hertz had established experimental evidence for the conversion of electron kinetic energy into excitational energy in mercury through inelastic collisions (which were dubbed inelastic "collisions of the first kind"), Klein and Rosseland showed that the reverse process could be energetically favorable, and Cario and Franck applied this idea to exciton transfer between two atoms - first publishing the idea [38], and then proceeding with the experiment [34]. In the case of interatomic collisional exciton transfer (also branded "collisions of the second kind" by Franck), de-excitation of the initially excited molecule would result in an energetically equal or lesser excitation in the second, with appropriately imparted kinetic energy making up the difference. Cario and Franck accordingly observed broadened thallium emission lines as a consequence of the Doppler effect [34]: kinetic energy imparted during the collisions resulted in a frequency shift corresponding to $v_2 = v_1(1 + \frac{v_1}{c}\cos\varphi)$, with the broadening of the thallium emission coming from the angular distribution of collisions relative to any observation point.

As noted in [39], it was shortly thereafter noticed by Franck and others [40],[41] that these "collisions of the second kind" between atoms and molecules -

that is, transfer of electronic energy as well as some amount of kinetic energy - were of greater probability when there was little kinetic energy imparted in the exchange. It is here that the term "resonance" begins to be used.

Several texts on the topic [42],[43] highlight that the first quantum mechanical theory of interatomic energy transfer [44] was immediately preceded by several other important developments: the work of Nordheim [45], Mensing [46], and Holtsmark [47] introduced classically or semi-classically considered dipole-dipole interactions. All were an attempt to explain much larger effective cross sections than were predicted by collisional theory alone. Thus, electronic multipole interactions were surmised to be the cause of this extended radius of interaction. Notably [47] and the later quantum-mechanical treatment of dipole-dipole interactions by Kallmann and London [44] constructed the framework to derive a $1/R^6$ transfer-efficiency relationship and critical distances - the distances at which nonradiative transfer would be 50% efficient - on the order of 10 nanometers.

In [44], Kallmann and London drew on the nascent work of Schrödinger [48] to derive the probability of energy exchange between two atoms with states in near-resonance, as a function of the difference of the electronic transition energies between the two atoms. As discussed in [42], the probability of transfer $|c^2|$ is oscillatory and was shown to be:

$$|c^2| = \frac{\beta^2}{1 + \beta^2} \sin^2 \left[\frac{\pi}{h} \sigma^* \sqrt{1 + \beta^2} t \right]$$

where $\beta = 2W_{12}/\sigma^*$ with W_{12} representing the overlap of the pre- and post- exciton exchange states from the dipole perturbation operator $W = \mu_1\mu_2/R^3$ acting on the acceptor with μ_1 and μ_2 representing the transition dipole moments of the donor and acceptor. σ represented the excited state energies of the interacting atoms with $\sigma^* = \sigma + W_{11} - W_{22}$ and the assumption that the ground state of both atoms were equal for simplicity. In [42], Clegg highlights this result and shows that by time averaging the probability of transfer one obtains:

$$|c^2|_{AVG} = \frac{1}{2} \frac{\beta^2}{1 + \beta^2} = \frac{1/2}{1 + \left(2 \frac{\mu_1\mu_2}{R^3\sigma}\right)^{-2}} = \frac{1/2}{1 + \left(\frac{R^6\sigma^2}{4(\mu_1\mu_2)^2}\right)} = \frac{1/2}{1 + \left(\frac{R^6}{R_0'^6}\right)}$$

with Clegg having defined $R_0'^6 = 4(\mu_1\mu_2)^2/\sigma^2$ to connect the result with Förster's

future work.

Of note is that this result is obtained only by considering a single de-excitation transition: in actuality there is a large distribution of possible transitions, especially in polyatomic molecules. As Förster notes in [33], in the case of complex fluorescent molecules, nuclear vibrations must also be considered, in addition to electronic transitions. What sets this derivation apart from later work, such as the solution-applicable quantum mechanical derivation by F. Perrin four years later [49], is that exact resonance is not a requirement - while a continuum of states is still not considered, the consideration of "near resonance" is more physically accurate as the

uncertainty principle would prevent two atoms from remaining in perfect resonance at all times.

Simultaneous pioneering work in the field was also undertaken by J. and F. Perrin during the 1920's and early 1930's. Förster mentions the work of both in his 1948 publication [22]. J. Perrin's research resulted in his similar observations of "transfert d'activation" as early as 1918 [50] whereby he surmised a vibrationally excited donor would induce excitation in a nearby acceptor through "une resonance secondaire." As noted in [51], it is not known when J. Perrin became aware of the work of Cario, Franck, and others concerning gas-phase collisional exciton transfer, and Perrin's initial model was derived directly from Faraday's law of induction [52]. Under this assumption, J. Perrin, together with Choucroun, surmised that that similar "excitation transfers at a distance" would be observed in viscous or rigid media [53], and in this work made connections to the experiments of Cario and Franck. In [51] it is noted that transformer-model of Perrin and Choucroun was originally proposed to explain a form of concentration-dependent fluorescence intensity quenching, which it would not be known until much later stemmed from formation of non-fluorescent aggregates rather than purely electronic intermolecular interaction.

F. Perrin's quantum mechanical derivation drew on the work of Kallmann and London [44], and London himself [54]. As highlighted in [55], Perrin's derivation considers a two-state system of identical molecules with a single exciton in the system. Thus the system is in a state of "pendulation" between the two

wavefunctions of the system represented as sums of the stationary-state inner products:

$$\begin{aligned}\psi_1 &= \frac{1}{\sqrt{2}} [\psi_E^1 \psi_G^2 + \psi_G^1 \psi_E^2] \\ \psi_2 &= \frac{1}{\sqrt{2}} [\psi_E^1 \psi_G^2 - \psi_G^1 \psi_E^2]\end{aligned}$$

where subscripts E,G represent the excited and ground states of particles 1 or 2 (denoted by superscript). In contrast to the derivation of London [54], Perrin considered one of the molecules to be in its excited state. London, on the other hand, was trying to quantify attraction between noble gas atoms and considered both in the ground state. Describing what have come to be known as "London dispersion forces," London, unlike Perrin, found an R^{-6} dependence on interaction energy from the same treatment. However, in London's case, this happened to coincide with Förster's result simply by chance: the first order perturbation on the energy of one particle from the intermolecular interaction is zero when both are in the ground state, and thus the second order term dominated. Considering one of the molecules to be excited, Perrin found the first order correction to the energy of one of the molecules to have an R^{-3} dependence.

At the time of Förster's 1948 publication, experimental evidence of intermolecular nonradiative energy transfer between fluorescent dyes in viscous media was considered largely in terms of fluorescence depolarization as a function of concentration in a single dye species, rather than the interspecies fluorescence

quenching more commonly considered in modern work. Förster includes in the paper a graph from the work of Feofilov and Svenshnikov [56], reproduced here in figure 1.3.1, depicting the fluorescence polarization of fluorescein in glycerine as a function of concentration, though it is noted that the effect was observed earlier [57],[58]. Polarization of fluorescence from molecules acting independently was expected to be a function of rotational freedom: in viscous solutions such as glycerine, rotational motions happen on a much longer timescale

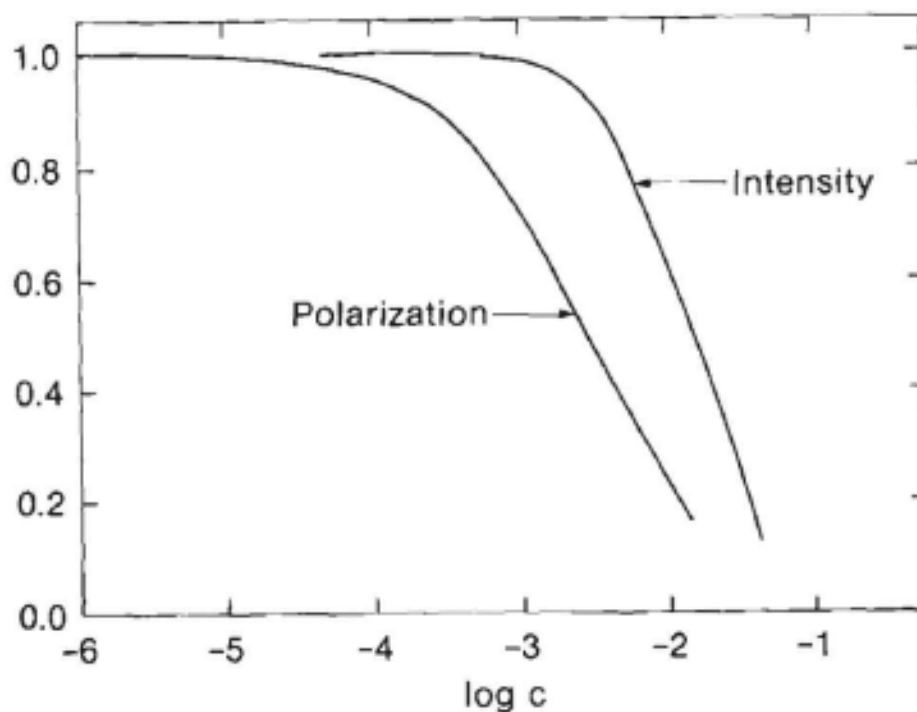


Figure 1.3.1: Semilog plot depicting fluorescence anisotropy and intensity of fluorescein in glycerine as a function of concentration. Depolarization of fluorescence is seen to happen in a much lower concentration regime than explainable by self-absorption of fluorescence. Reproduced from [22].

than fluorescence decay, and excitation with polarized light should result in similarly polarized emission. Many absorption and remission events might extend the fluorescence timescale, but for that to occur the optical density of the solution would be large enough for self absorption effects to be seen in the fluorescence intensity measurements as a function of concentration. In fact, depolarization happens in a much lower concentration regime - and nonradiative exciton transfer was expected to be the culprit. Application of Perrin's theory, however, predicted the depolarization occurring at concentrations an order of magnitude lower than where it actually did.

In the decade and a half between Perrin's 1932 paper and Förster's 1948 publication, several other well known theorists considered the issue of exciton transfer from various perspectives. As described in [55] for example, Teller, Oppenheimer, and Franck attempted to apply the theory to exciton transfer between Chlorophyll molecules in photosynthetic units, an idea which, while actually correct, went without validation for some time because of several erroneous assumptions. The critical connection between the early quantum mechanical treatments of nonradiative exciton transfer and Förster's work, however, was that of Dirac's work [59]. In what Fermi would later call "Golden Rule No. 2" in a series of published lectures at the University of Chicago [60] (thus popularizing the relation as "Fermi's Golden Rule"), Dirac determined the probability per unit time (W) of a molecule's transition from its initial state to an ensemble of final states upon perturbation with an oscillating Hamiltonian (H) (for example, a molecule in its ground state absorbing a photon):

$$W = \frac{2\pi}{\hbar} \left| H_{fi} \right|^2 \frac{dn}{dE}$$

where H_{fi} is taken to be $\langle f|H|i\rangle$, the matrix element of the perturbation which causes the transition from the initial to final state, and with dn/dE representing the density of the final state energies. In section three of [22] ("Mechanismus des Energieübergangs"), Förster extends this idea to apply to "donor-acceptor" interactions, with the perturbation Hamiltonian stemming from the fluorescence dipole of the initially excited molecule, a calculation which can itself be averaged over an ensemble of initial states. Section four, "Zusammenhang mit den Spektren," provides similarly important insight by relating the thermal equilibrium distribution of the excited state vibrational motion to the number of photons emitted per unit time per molecule and thus the fluorescence spectrum (with a similar parallel drawn between the frequency dependence of the absorbance coefficient and the thermal equilibrium distribution of the ground state). Thus, Förster made the connection between exciton transfer probability (and thus donor-acceptor pair distance) and easily measurable physical quantities, resulting in the now famous formulae:

$$\kappa_T = \frac{1}{\tau_D} \left(\frac{R_0}{R} \right)^6 \quad (1.3.1)$$

with R_0 calculable from:

$$R_0^6 = \frac{9000 \ln(10) \kappa^2 \phi_d}{128 \pi^5 N n^4} \int_0^\infty F_d(\lambda) \varepsilon_a(\lambda) \lambda^4 d\lambda \quad (1.3.2)$$

where κ_T is the distance-dependent nonradiative transfer efficiency, τ_D is the fluorescence lifetime of the donor in the absence of an acceptor, ϕ_d is the normalized donor fluorescence per unit wavelength, $\varepsilon_a(\lambda)$ is the molar extinction coefficient of the acceptor between λ and $\lambda + d\lambda$, n is the refractive index of the host medium, and N is Avogadro's number. κ^2 , the dipole orientation factor, is given by [23]:

$$\kappa^2 = (\cos \theta_T - 3 \cos \theta_D \cos \theta_A)^2$$

with θ_T denoting the angle between the transition dipole moments of the donor and the acceptor, and $\theta_{D,A}$ representing the angle between the donor or acceptor transition dipole moments and the vector between the donor and acceptor.

While it seems rather straightforward to accept that an excited donor will remain in an excited state for less time when its exciton is readily transferred to an acceptor, as discussed in [61], it is interesting to classically consider the implications of an increased donor decay rate on the presence of an acceptor - in other words, how a passive absorber can affect a donor's fluorescence lifetime. Such consideration also gives insight into the classical derivation of the R^{-6} transfer rate dependence. When considering a molecule's fluorescence dipole as a classical Hertzian electric dipole in a vacuum, it will emit \vec{E} and \vec{B} fields whose real parts are given in Gaussian units by [62]:

$$E = k^2 p \frac{\cos(kr - \omega t)}{r} (\hat{\mathbf{r}} \times \hat{\mathbf{p}}) \times \hat{\mathbf{r}} + p \left[\frac{\cos(kr - \omega t)}{r^3} + \frac{k \sin(kr - \omega t)}{r^2} \right] [3(\hat{\mathbf{p}} \cdot \hat{\mathbf{r}})\hat{\mathbf{r}} - \hat{\mathbf{p}}]$$

$$\mathbf{B} = k^2 p \left[\frac{\cos(kr - \omega t)}{r} - \frac{\sin(kr - \omega t)}{kr^2} \right] (\hat{\mathbf{r}} \times \hat{\mathbf{p}})$$

where p is the magnitude of the dipole $k = \omega/c$. What is noted in [61] however, and shown in detail in [62], is that time-averaging the Poynting vector (energy flux) in both the near and far zone yields:

$$\langle S \rangle = \frac{p^2 \omega^4 \sin^2(\theta)}{8\pi c^3 r^2} \hat{\mathbf{r}}$$

where the average divides out time from the Poynting vector to yield intensity. This can be integrated over a spherical surface to yield a total radiated power of:

$$P = \oint_r \langle S \rangle \cdot d\mathbf{A} = \frac{p^2 \omega^4}{3\pi c^3}$$

Given that the Poynting vector may be defined as $\mathbf{S} = \frac{c}{4\pi} (\mathbf{E} \times \mathbf{B})$, its time average can be expressed as $\langle S \rangle = \frac{c}{8\pi} E_0^2 \hat{\mathbf{r}}$ with E_0 denoting the amplitude of the electric field. This is evident without further derivation in the 'radiation' zone by considering the $1/r$ terms in the \mathbf{E} and \mathbf{B} fields and noting that here $|\mathbf{B}| = |\mathbf{E}|$ (as in the case of a monochromatic plane wave) and that $[(\hat{\mathbf{r}} \times \hat{\mathbf{p}}) \times \hat{\mathbf{r}}] \times (\hat{\mathbf{r}} \times \hat{\mathbf{p}}) = \hat{\mathbf{r}}$; it is also shown to hold in the near zone over a full cycle of oscillation in [62] by performing the cross product and time averaging. An absorber with cross section σ , then, will absorb $P_A = \frac{c}{8\pi} E_0^2 \sigma$ as noted in [61]. Although through a less trivial explanation, it can also be shown that the power absorbed by an acceptor in the near zone scales with the square of the electric field amplitude when averaged over an arbitrary period of time,

without considering an arbitrary cross section σ : by taking from Poynting's theorem that the power absorbed by an acceptor is the rate at which work is done on its charges, by conservation of energy $P_A = \int \mathbf{J} \cdot \mathbf{E} dV = -\frac{1}{2} \int \text{Re}\{\mathbf{J}_A^* \cdot \mathbf{E}\} dV$. Noting that \mathbf{j}_A , the current density induced in an acceptor, can be rewritten in terms of its induced dipole moment $\mathbf{j}_A = -i\omega\boldsymbol{\mu}_A\delta(\mathbf{r} - \mathbf{r}_A)$, where the induced dipole is given as $\boldsymbol{\mu}_A = \overleftrightarrow{\alpha}_A \mathbf{E}$ (and confining polarizability to a fixed direction to eliminate the need to consider the polarizability tensor) another donor electric field term is introduced and a comparable dependence is thus shown to hold ([63], section 8.6). Putting all of this together, and looking at the behavior of the electric field vector in the near zone over the course of an oscillation of the dipole, it can be seen from the plots given in figure 1.3.2 [62] that in this region a large portion of the electric field is characteristic of an electrostatic dipole, rather than an outwardly propagating plane wave. As a consequence, a large portion of the time dependence of the Poynting vector has terms which oscillate like $\cos(kr - \omega t) \sin(kr - \omega t)$. These time average to zero over a complete cycle, and imply a "recycled" energy flow in the near zone such that when an absorber is placed in this region, it absorbs energy that would otherwise not be radiated, thus increasing the donor's decay rate. It is similarly noted by [61] that:

$$E_0^2 \propto \frac{k^4}{r^2} + \frac{k^2}{r^4} + \frac{1}{r^6} \propto k^4 \left(\frac{1}{r^2} + \frac{1}{k^2 r^4} + \frac{1}{k^4 r^6} \right) \propto \frac{1}{\lambda^4 r^2} \left(1 + \left(\frac{\lambda}{r} \right)^2 + \left(\frac{\lambda}{r} \right)^4 \right)$$

with $k = \omega/c = 2\pi/\lambda$. In the near zone then, when $r \ll \lambda$, the r^{-6} term dominates the

square of the electric field and thus the power absorbed scales with the fourth power of wavelength and the inverse sixth power of distance.

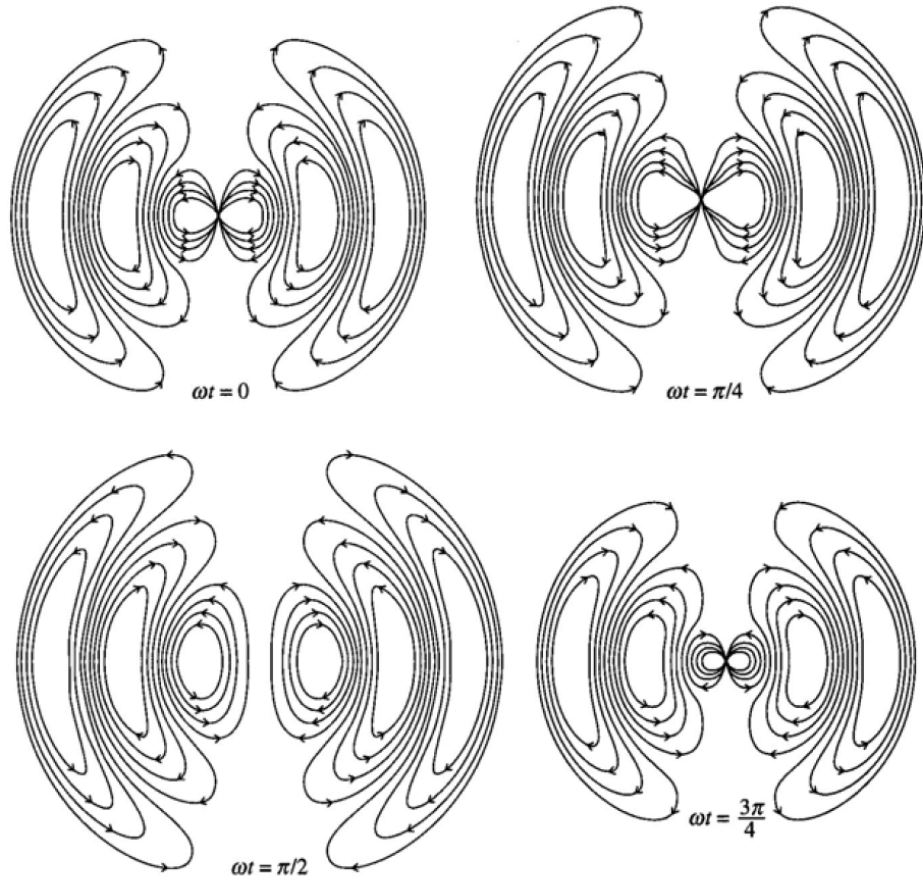


Figure 1.3.2: Behavior of the electric field vector in the near-field region of a Hertzian dipole. Field patterns are distinct from those in the radiation zone. Reproduced from [62].

Chapter 2

2.1 Doctor-bladed sample preparation: Determining FRET concentration regime

DCM ([2-[2-[4-(dimethylamino)phenyl]ethenyl]-6-methyl-4Hpyran-4-ylidene]-propanedinitrile) (Exciton) and Lumogen Red 305 (BASF) were used as obtained (structures shown in figure 1.2.1). Luminescent inks were prepared from a mixture of the as-received powdered dyes, polymethylmethacrylate (Spectrum Chemical Co., 350k MW), and toluene. To achieve global film uniformity across a range of dye to host polymer concentrations, a standard 13.3% PMMA:Toluene weight ratio was established for all inks. The film deposition was performed using an Industry Tech Auto Draw III automatic drawdown machine. The machine draws a rod across a slide at constant pressure and velocity to produce a film. Film thickness was set using a single layer of Scotch 810 magic tape. The films were deposited on 3"x1" quartz glass microscope slides. The films themselves were determined to be approximately 5 microns in thickness, and examples are shown in figure 2.1.1.

A Stellar Net Thin Film Measurement System, including an SL-1 Filter, a CXR-SR-25 BW-16 Spectrometer, and a Wave NIR-25 InGaAs BW Spectrometer, was used measure absorption spectra. A Perkin Elmer Instruments LS45 Luminescence Spectrometer was used to measure the surface emission of the films, by placing the samples in the spectrometer's "front surface" accessory. The excitation beam strikes at 60 degrees to the film's normal, and emission is collected at 30 degrees relative to the film normal. Film thickness measurements were determined from a

Dektak profilometer and found to agree with the known molar absorption coefficient from literature [27].

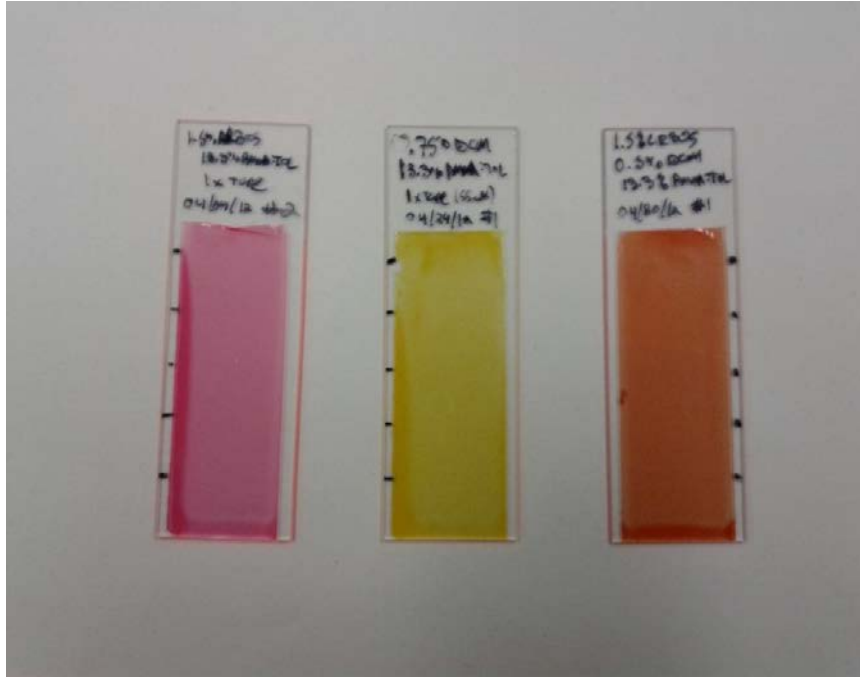


Figure 2.1.1: 0.75% LR305 film in PMMA, 0.5% DCM film in PMMA, 0.75% LR305/0.5% DCM blend (left to right, percentages by weight).

2.2 LSC device sample preparation

A second experiment was devised to measure the effect of FRET on waveguide transport losses. A preliminary result was achieved by taking external quantum efficiency data from side-mounted PV modules mounted on two LSC devices. As FRET efficiency depends on the distance between chromophore molecules and thus concentration, in order to experimentally determine the benefit of FRET, it seemed easiest to compare high and low concentration samples of the same total absorbance

(absorption held constant by compensating for increased concentration by reducing thickness), with the same donor:acceptor concentration ratio (in this case, a 1:1 molar ratio) in each sample. This would require the thickness of the sample to be varied over a wide range to maintain a constant optical density, an outcome for which doctor-blading was no longer a suitable process. For this experiment, an entirely different preparation process was needed. Access to a vacuum-type hot press was obtained, with the goal of constructing variable-width LSC devices of the structure shown in figure 2.2.1.

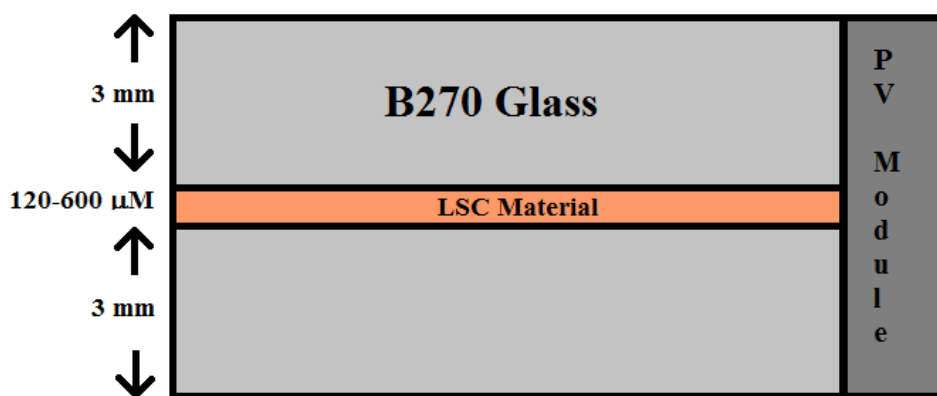


Figure 2.2.1: Sample LSC device construction (not drawn to scale). An absorbing LSC layer (polymer doped with dyes) is optically sandwiched between two 3 mm glass plates. The polymer is index matched to the glass.

This structure is similar to those noted in previous publications on the subject, as described in [17] and [21]. Various problems however, largely related to the heating process and high melting point of PMMA, prevented the use of DCM and LR305 (further discussed in section 3.3). In order to achieve the desired experimental goals, proprietary dyes were obtained and pressed in pure ethylene-vinyl acetate

(EVA), without further additives. The spectroscopic and properties of the materials used for this experiment are discussed in section 3.3. The vacuum-type press was heated to 80 degrees Celsius and the samples were pressed to the appropriate thickness under <100 Pa ambient pressure. The vacuum was necessary to remove bubbles from the EVA caused by outgassing during heating [64]. The total area of the devices was approximately 70 cm^2 . Thickness and concentration of the LSC layer were varied by a factor of 5 (0.25% total dye:host polymer concentration, 120 microns for “high density” sample, 0.05% concentration, 600 microns thickness for the “low density” sample) - thus the overall waveguide thickness changed by less than 10% (6.12 mm to 6.6mm). The inactive edges of the devices were then coated with non-reflective absorbing ink, to keep light from reflecting from inactive edges and artificially inflating measured efficiency. Commercially available crystalline silicon cells, whose electrical properties are discussed further in section 3.3, were optically coupled to the active side using UV-curable optical adhesive, and cured for 3 minutes under 3-sun UV conditions. During the curing process, the LSC portion of the devices were covered with a reflector to prevent photodegradation of the LSC material. The resulting devices, shown in figure 2.2.2 were observed to be free of defects and to have comparable optical densities. The test methods and results are further discussed in section 3.3.

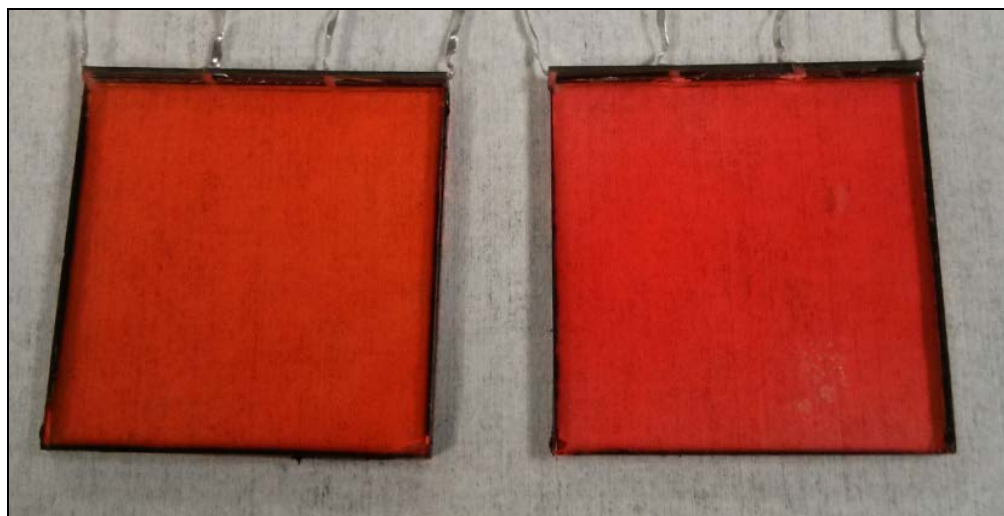


Figure 2.2.2: "Low" (left) and "high" (right) density LSC samples, with coupled PV modules and inactive edges coated with absorbing ink. The absorbing layer of the low density sample is 0.05% dye:polymer (by weight) and 600 microns thick. High density sample absorbing layer is 0.25% dye:polymer and 120 microns thick.

Chapter 3

3.1 Establishing FRET dominance as a function of dye:host concentration

BASF Lumogen Red 305 and DCM dyes fluoresce in the yellow-red visible range, with emission peaks at 604nm and 555 nm, respectively, when embedded in a PMMA polymer matrix. Both have been considered for use in LSC applications because of their broad Stokes Shifts and high quantum yields. In addition to its promising fluorescence overlap with the absorption of LR305, DCM was investigated as a companion dye to Lumogen Red 305 because its absorption peak compliments a dip in the absorption spectrum of LR305, as is shown in figure 3.1.1.

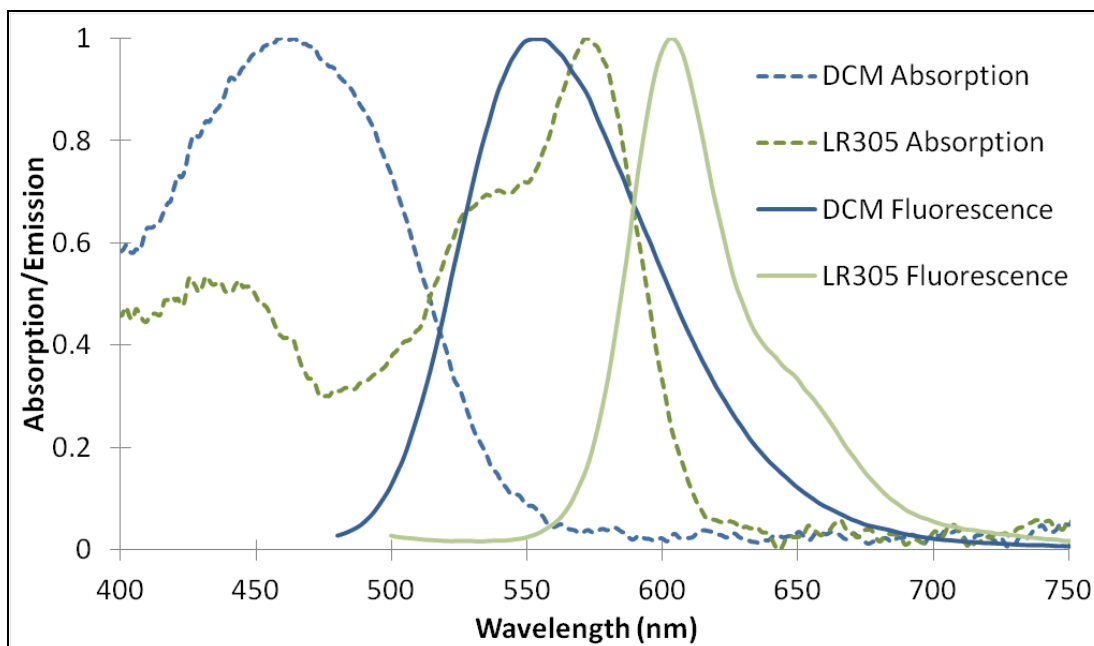


Figure 3.1.1: Normalized absorption and emission spectra of LR305 and DCM dyes in PMMA.

LR305 has been shown to be capable of near unity quantum yield in PMMA [65]. It was similarly noted in [27] that the molecular emission spectrum of LR305 was seen to shift between 597 nm and 611 nm (with no change in quantum yield) as the excitation wavelength was varied between 490 nm and 620 nm. The authors noted that this could be explained by the redshifted absorption and emission of dimer or trimer aggregates contributing to emission at longer excitation wavelengths. Attempts to replicate this effect in the course of the work presented here were unsuccessful; with 0.1% 5 micron films and optical densities sufficiently low to neglect self absorption effects [23], a consistent 604 nm emission peak was observed between 440 and 590 nm excitation with 3 nm entrance and exit slit bandwidth, as shown in figure 3.1.2.

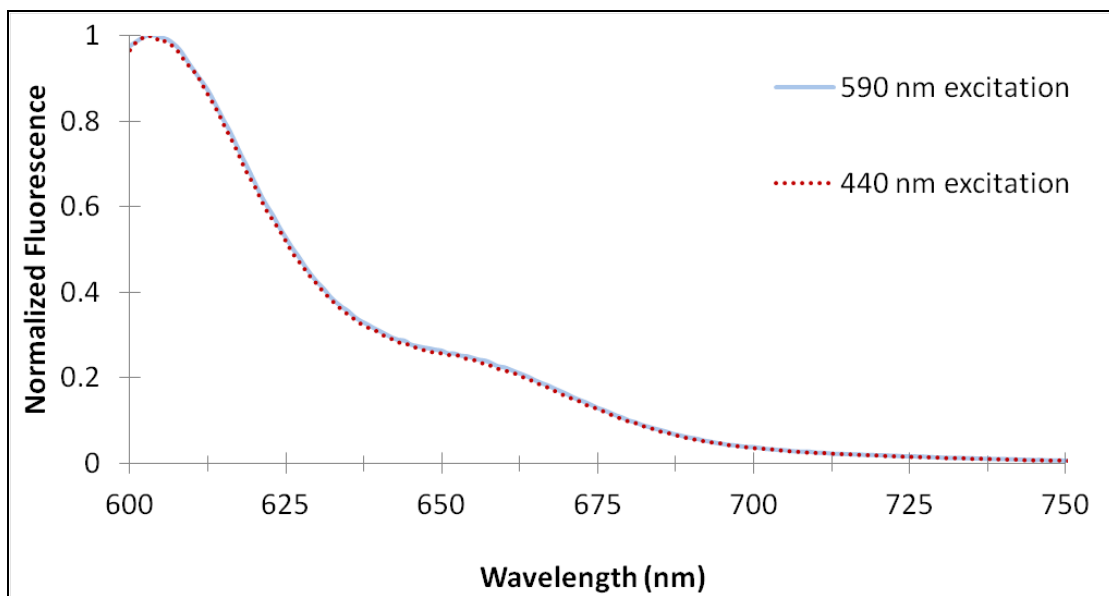


Figure 3.1.2: Emission spectra of spin-cast, low optical density LR305 films in PMMA. No change in emission is observed between 440 nm and 590 nm excitation.

Differences in the experimental setup and film preparation method (doctor blading a toluene:polymer:dye mixture versus casting thick molds) required the use of concentrations at least an order of magnitude greater than in [27]. Thus, it is possible that FRET homotransfer is responsible for an averaging effect of the fluorescence at all excitation wavelengths, although a simpler explanation would be differences in spectrometer calibration and the absence of the aggregates in our films - either due to differences in received dye batches, or perhaps from differences in the film preparation method.

In both the stacked and blended films, the additive absorbance spectra are seen, as would be expected from the Beer-Lambert law. This is shown in figure 3.1.3. The result of interest, however, is seen when multiple fluorescing species are

combined into a single film. The surface emission spectra of single dye LSC films, blended LSC films, and stacked single dye films were compared. The results are shown in figure 3.1.4. The data shown here are taken from films of like composition: approximately 5 micron thick doctor bladed films on silicate glass, with PMMA as the host polymer as described in section 2.1. The single dye DCM and LR305 films used in figure 3.1.3 have dye:polymer ratios of 0.5% and 0.75% by weight, respectively. The blended dye film has the same amounts of each dye as in the single films, that is: 0.5% DCM:PMMA and 0.75% LR305:PMMA by weight, for a total dye concentration of 1.25% dye:polymer. Stacked film emission data were taken by placing the two single dye films on top of one another, with the LR305 film above the. The film emission spectra were taken with 460nm excitation, optimized for absorption by DCM.

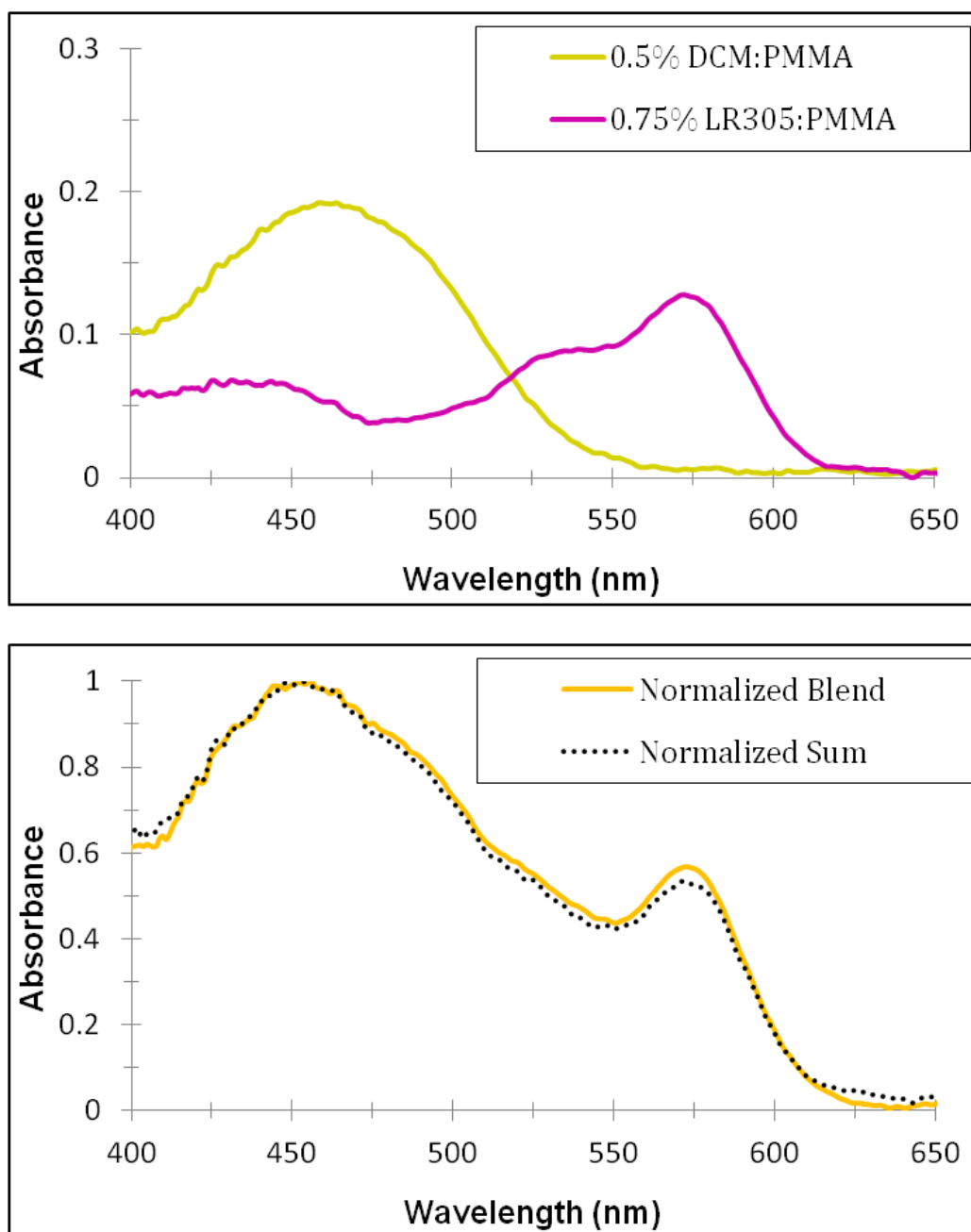


Figure 3.1.3: Comparison of 0.5% donor (DCM), and 0.75% acceptor (LR305) wavelength dependent optical density (top). Blended film absorbance of same concentrations (1.25% total dye) is compared with a sum of the optical densities at each wavelength (bottom). All optical density (absorbance) measurements taken at normal incidence.

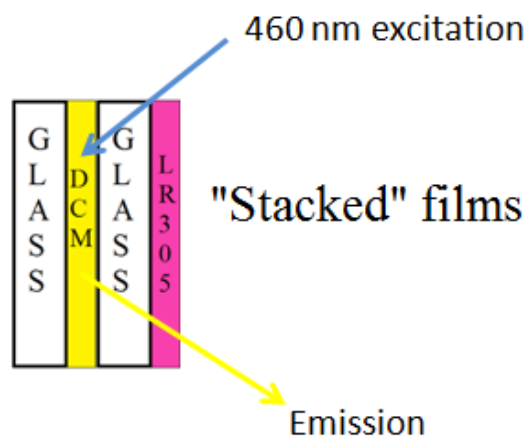
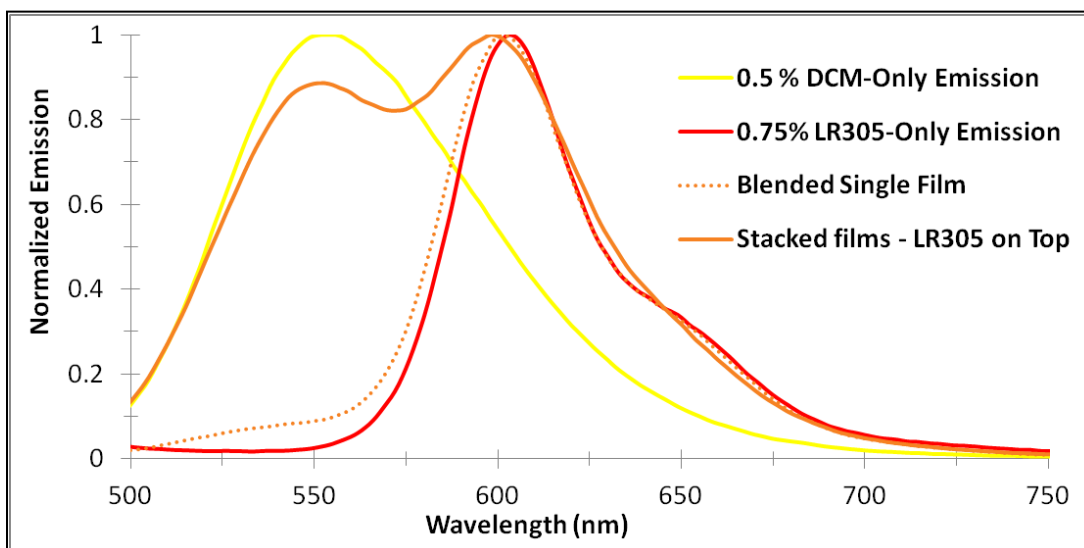


Figure 3.1.4: Comparison of the emission spectra of stacked and blended LR305/DCM 0.75%/0.5% PMMA films when excited with 460 nm light. The "blended single film" is a single layer containing both 0.75% LR305:PMMA and 0.5% DCM:PMMA. "Stacked" films (illustrated above) are comprised of single-dye films (0.75% LR305:PMMA on top, 0.5% DCM:PMMA on the bottom) physically stacked on top of one another, with the LR305 "acceptor" film closer to the detection and excitation source. As such, any DCM emission would necessarily pass through the full LR305 optical density. Despite this, the stacked films show strong DCM fluorescence while the blend shows almost none.

In the "stacked" setup (figure 3.1.4), any DCM emission would necessarily pass through the LR305 film's entire optical density before being detected. The 0.75% LR305 film was measured to have a peak optical density of 0.166. In [27], LR305 was found to have a Napierian (natural logarithm) peak absorbance coefficient of $0.101 \text{ ppm}^{-1} \text{ cm}^{-1}$ (where a 'part per million' was defined as 10^{-4} percent by weight in the host), which converts to an optical density of approximately 0.0439 absorbance units per percent by weight per micron thickness, agreeing with the 5 micron thickness measurement.

Although a small portion of the DCM emission is absorbed passing through the LR305 film, the stacked film emission stands in stark contrast to that of the blend. Likewise, the emission spectrum of the stacked films under 460 nm excitation closely matches their independent superposition (figure 3.1.4), however the blend shows almost entirely acceptor (LR305) emission. It should also be noted that DCM emission in the blend will, on average, pass through half the optical density of the LR305 film, assuming a uniform distribution of dopants, further highlighting a non-radiative quenching mechanism in the blend.

As another example, consider figures 3.1.5 and 3.1.6. Figure 3.1.5 depicts a 0.625% DCM:PMMA film emission under 460 nm excitation with various amounts of LR305 dye added, while 3.1.6 depicts the absorption spectra of the added LR305 dye as well as DCM's normalized fluorescence spectrum. While a cursory glance at figure 3.1.5 suggests that DCM emission is simply being absorbed as more LR305 is added,

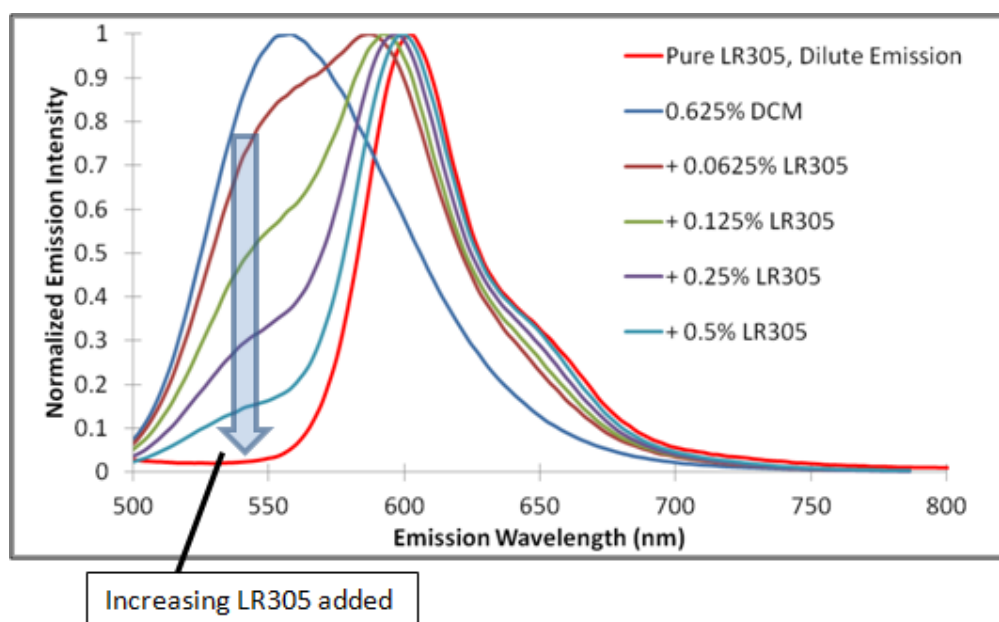


Figure 3.1.5: Normalized emission spectra of 0.625% DCM:PMMA films with varying levels of LR305 dye added. 460 nm excitation used in all cases. DCM emission is seen to be quenched with increasing LR305, however optical density of added LR305 is much lower than necessary to explain DCM fluorescence quenching.

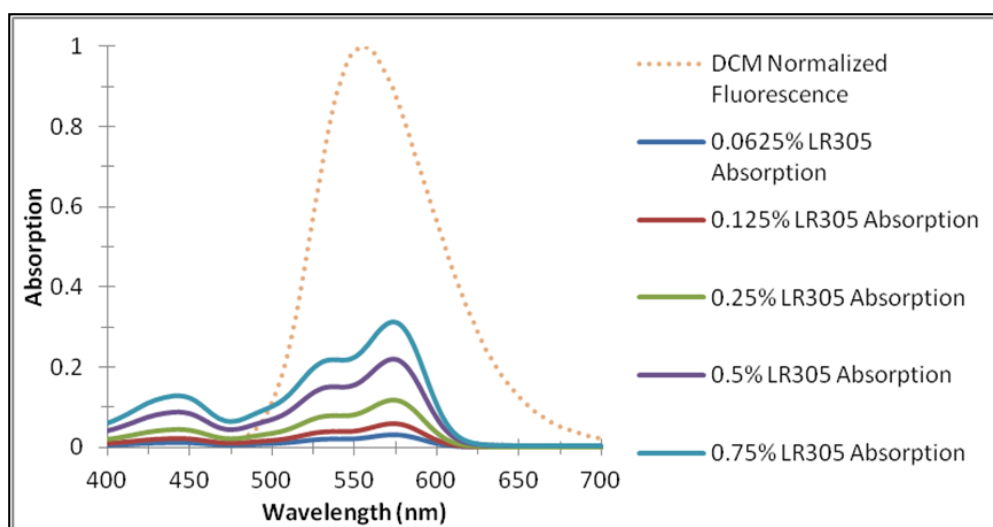


Figure 3.1.6: Absorption spectra of LR305 films. Compare with figure 3.1.5. A 5 micron thick 0.5% LR305 film has approximately 17% absorption at 555 nm, but mixing 0.5% LR305 into a 5 micron thick DCM film quenches over 85% of its 555 nm fluorescence (as seen in figure 3.1.5).

figure 3.1.6 reveals that the optical density of the associated dye addition is too low to account for the phenomenon. Additionally, emission of DCM is not merely quenched - the emission intensity of LR305 is correspondingly increased. Consider the fluorescence intensity of LR305's 604 nm peak in a 0.75%, 0.5% LR305/DCM blended film when compared with a film containing LR305 alone (figure 3.1.7) as the excitation wavelength is swept across the absorption range of both LR305 and DCM. Without the DCM present, the LR305 peak emission intensity scales with the LR305's absorption spectrum as a function of excitation wavelength. Below 540 nm, the benefit from the added absorption of DCM is clearly seen. A corresponding enhancement is also seen in the LR305 emission. As can be seen in figure 3.1.8, samples of LR305 films are compared under 460 nm excitation, with different amounts of DCM added into the film. LR305 has a dip in its absorption in this excitation region, and as a result has comparatively weak fluorescence from 460nm excitation. While radiative energy transfer would also increase LR305 fluorescence, this would be subject to the fluorescence quantum yield of DCM and the absorption of LR305 across DCM's fluorescence range. Noting from figure 3.1.8 that adding 0.0625% DCM:PMMA to a 0.75% LR305 film increases the films 460 nm absorption by almost exactly 50%, and that a corresponding increase in fluorescence intensity under 460 nm excitation of almost exactly 50% is also observed, a non-radiative transfer mechanism is similarly demonstrated. Even very small amounts of DCM can appreciably increase emission response, with virtually no DCM emission detectable.

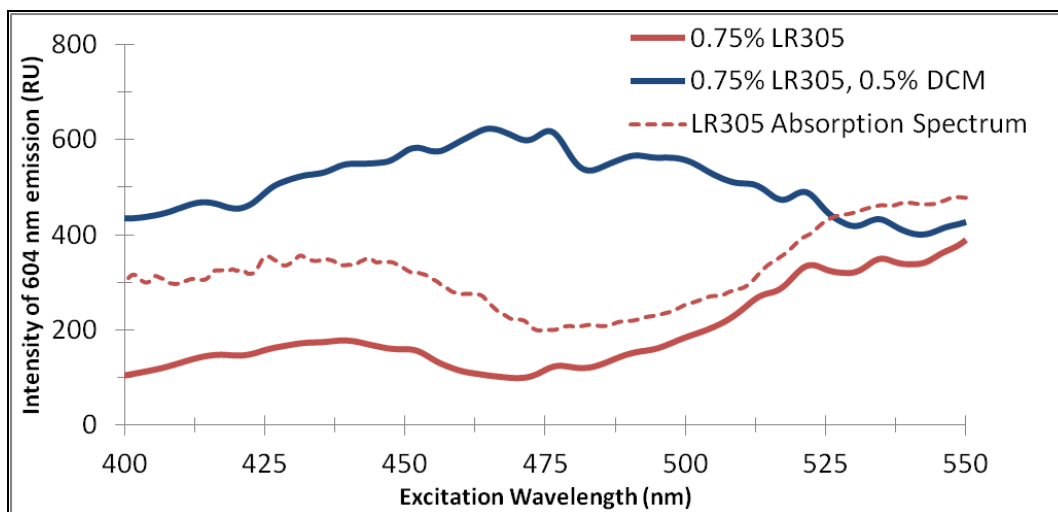


Figure 3.1.7: 604 nm emission intensity as excitation wavelength is swept across the absorption range of LR305 and DCM. The blended film shows enhanced LR305 emission response in the range of DCM's absorption. Intensities given in relative but arbitrary units (RU).

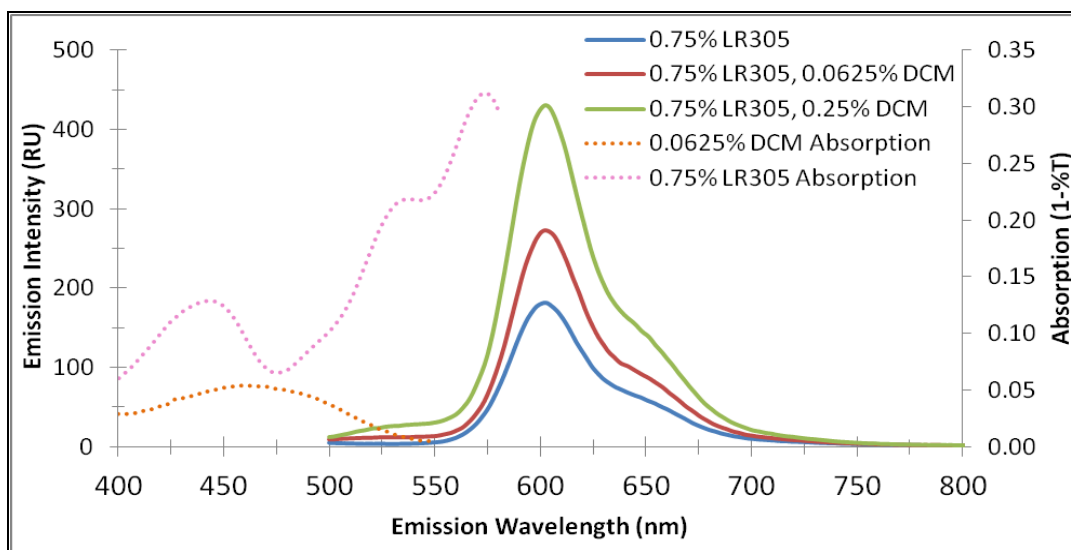


Figure 3.1.8: Emission spectra of 0.75% LR305 films under 460 nm excitation. Absorption spectra of 0.75% LR305 and 0.0625% DCM films are also shown. The addition of 0.0625% DCM increases the 460nm absorption of the LR305 film by almost exactly 50%. A corresponding enhancement in LR305 emission is also seen (by integrated spectrum). 0.75% LR305 5 micron films absorb <30% at their peak (and considering entire optical density of the film), and DCM has a quantum yield of 76% in PMMA. Emission enhancement therefore exceeds that possible from radiative transfer. Intensities given in relative but arbitrary units.

Radiative energy transfer, or emission of a photon by a donor chromophore and its subsequent reabsorption by the acceptor, can occur over macroscopic distances. The large spectral overlap between the absorption spectrum of LR305 and DCM's emission suggests that radiative energy transfer will occur to some extent if the dyes are placed in close proximity, however, when the relative intensities of the DCM and LR305 fluorescence peaks are compared between blended dye films and the stacked films (figure 3.1.4), as well as when fluorescence quenching is compared with film optical density (figures 3.1.5, 3.1.6) the radiative processes are shown not to be the dominant energy transfer mechanism. As the dyes are confined to a rigid polymer matrix, collisional energy transfer is not expected to play any role. At very high concentrations, with intermolecular distances of less than 20 angstroms, Dexter Electron Transfer (also referred to as exciton diffusion), may play a role [66]. The mechanism stems from a physical overlap of donor and acceptor electron wavefunctions. It is likely that considerations of DET are outside the scope of the samples studied in this work, as FRET does not require the physical overlap of electron wavefunctions, and for samples with appreciable spectral overlap and random orientations, FRET is expected to work on distance scales generally up to an order of magnitude greater. As such, Dexter Electron transfer is not expected to be the dominant mechanism in the concentration regimes surrounding the Förster critical distance, and we instead consider only Förster's formulation in terms of the overlap of the absorption and emission spectra, which is observed to be large in the 525-575 nm range, as seen in figure 3.1.1.

As discussed in section 1.3, a useful figure of merit in Förster theory is the critical distance R_0 , at which the rate of energy transfer from the donor to the acceptor fluorophore is equal to the rate at which the donor will decay from its excited state in the absence of the acceptor. This can also be described as the donor-acceptor pair distance at which energy transfer is 50% efficient, and is given as described by equation 1.3.2. κ^2 , the dipole orientation factor discussed in section 1.3, is here taken to be 0.476, which has been shown to be the value of the orientation factor for randomly distributed donor and acceptor molecules in a rigid polymer matrix [67]. Taking a donor quantum yield of 76% for DCM (ϕ_d), and using an overlap integral numerically determined to be $6.15 \times 10^{-14} \text{ cm}^3 \text{ M}^{-1}$ from the data used to generate figure 3.1.1, a critical FRET distance of 39.8 Å between DCM and LR305 in PMMA is obtained.

Using these relationships, as well as the relative fluorescence intensities of DCM with and without LR305 present, it is possible to estimate average donor-acceptor pair separation as a function of dye concentration. To this effect, total dye:polymer concentration was varied at two fixed LR305:DCM ratios: 1:2 LR305:DCM and 3:2 LR305:DCM (by weight). Fluorescence intensity of the blends is compared against films containing only the donor at several representative concentrations in figures 3.1.9 and 3.1.10.

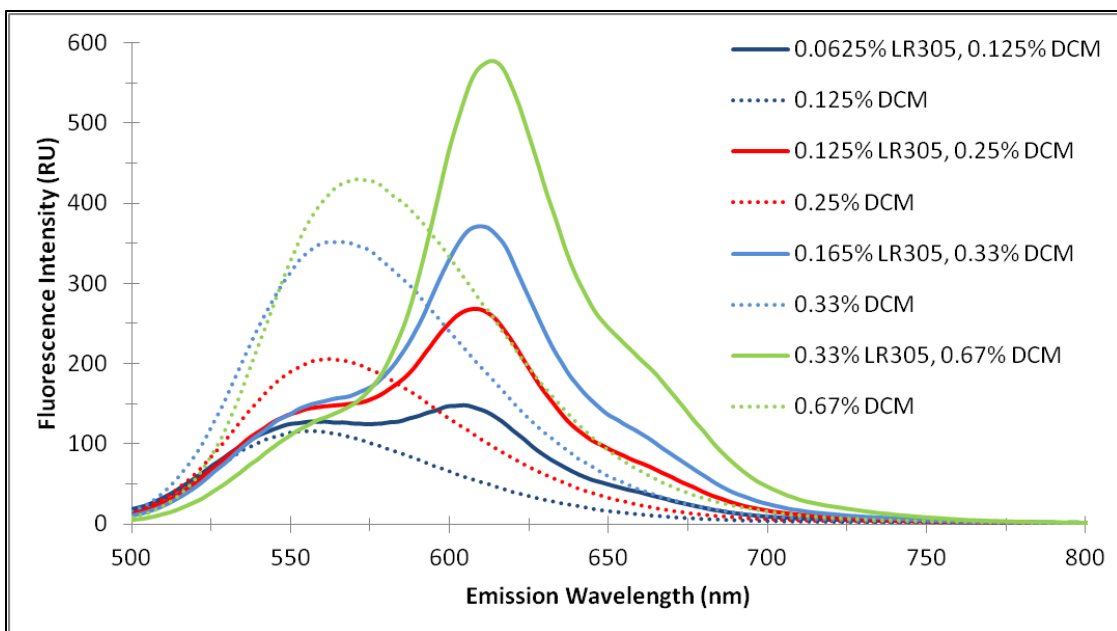


Figure 3.1.9: Sample non-normalized emission profiles of 1:2 weight ratio LR305/DCM films under 460 nm excitation. DCM emissions is quenched as concentration rises. Intensities given in relative but arbitrary units (RU).

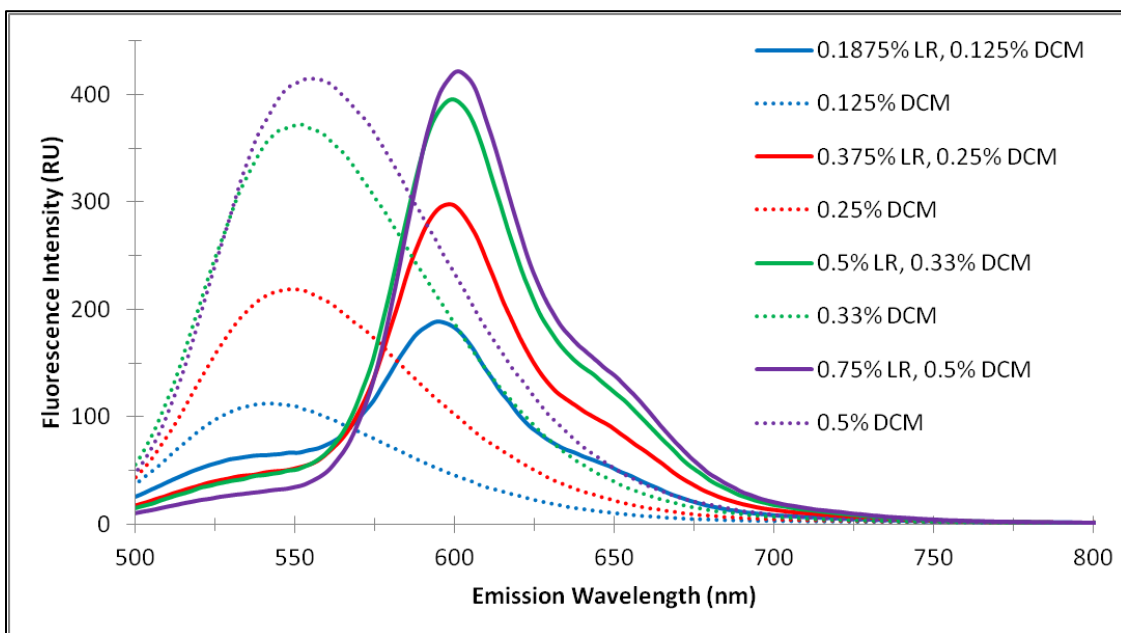


Figure 3.1.10: Sample non-normalized emission profiles of 3:2 weight ratio LR305/DCM films under 460 nm excitation. The same effect is again seen.

By comparing the ratio of the donor fluorescence intensity in the presence of the acceptor to its intensity in the acceptor's absence, it is possible to estimate the transfer efficiency from Förster's relations:

$$E = 1 - \frac{F_{DA}}{F_D} \quad (3.1.1)$$

Using the critical distance, R_0 , calculated from spectroscopic data and equation 1.3.2, we can then estimate the donor-acceptor separation according to [23]:

$$E = \frac{R_0^6}{R_0^6 + r^6} \quad (3.1.2)$$

This dependence has also been experimentally confirmed: [68],[69] are some examples. Equation 3.1.2 can be derived by considering the transfer efficiency to be the ratio of excitons non-radiatively transferred to the acceptor to the total amount absorbed per unit time:

$$\frac{\text{PhotonsTransferred}}{\text{PhotonsAbsorbed}_{\text{Donor}}} = \frac{\kappa_T(r)}{\tau_D^{-1} + \kappa_T(r)} \quad (3.1.3)$$

where $\kappa_T(r)$ is the non-radiative transfer rate first defined in equation 1.3.1 and τ_D is the unquenched donor lifetime. Förster's theory predicts an R^{-6} dependence on transfer efficiency; using the 39.8 Å R_0 calculated from the spectral overlap and efficiencies calculated from equation 3.1.1 and DCM peak fluorescence intensity, it is possible to plot pair distance as a function of concentration. It is encouraging to see that the $-1/3$ power relationship between molecular spacing and concentration

expected from dimensional analysis is approximately recovered at both tested donor:acceptor ratios (figure 3.1.11). Combining both donor-acceptor ratios and looking at calculated donor-acceptor pair distance as a function of acceptor concentration is also useful; acceptor interaction with a "nearest" donor is substantially more likely than interaction with more distant donors. Similarly, donor-donor nonradiative homotransfer has a substantially lower probability in the concentration regime surrounding the donor-acceptor critical distance, and therefore calculated D-A pair distance is likely largely a function of acceptor concentration.

The fitted curves plotted in figures 3.1.11 and 3.1.12 are least squares power law fits with the exponent fixed at $-1/3$ such that the leading coefficient of the form $separation = A\{concentration\}^{-1/3}$ is fit to the data. A power law fit based on intensity measurements will be extremely prone to fixed percentage intensity uncertainties in the lower concentration regime. Meaningful analysis of quantitative fits in future work should optimally compare fluorescence anisotropy and donor fluorescence lifetime against intensity results. Because of many of the considerations discussed in work such as that of [25], the fits provided here are meant as a purely qualitative result.

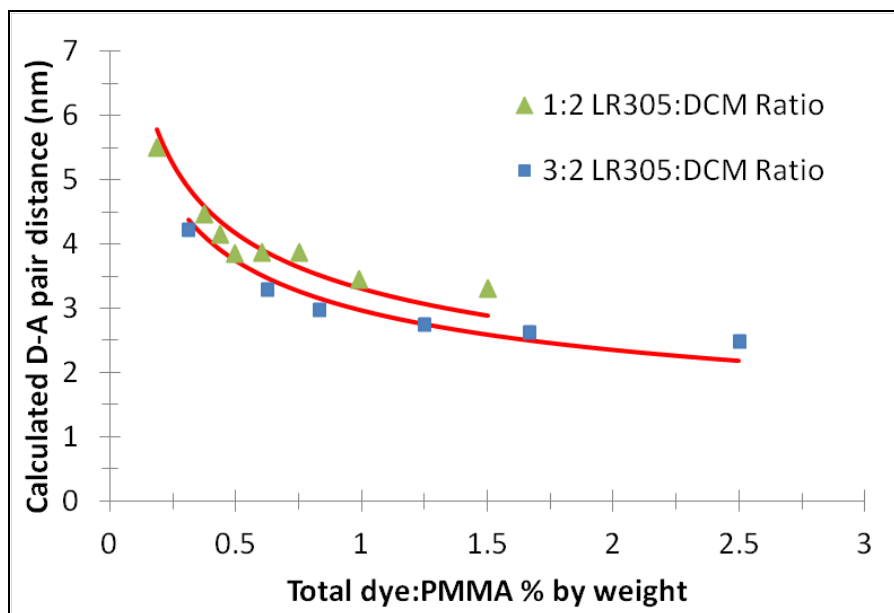


Figure 3.1.11: Recovery of approximate $\{\text{concentration}\}^{-1/3}$ intermolecular distance from least squares fit of leading coefficient to calculated D-A pair distances.

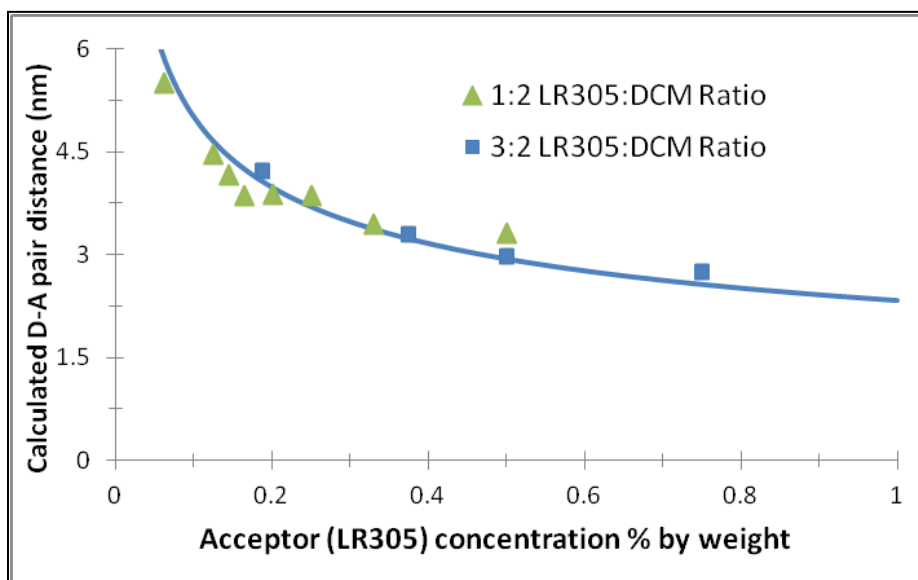


Figure 3.1.12: Plot of calculated donor-acceptor pair distance as a function of acceptor concentration with donors added in different ratios. Given the R^{-6} transfer probability dependence, acceptor interaction with a "nearest" donor is substantially more likely than interaction with more distant donors. Similarly, donor-donor non-radiative homotransfer has a substantially lower probability in the concentration regime surrounding the donor-acceptor critical distance.

3.2 FRET, AM1.5 Absorption, Film Self Absorption

Even assuming unity quantum yield, no emission re-absorption, and no scattering from the host material, LSCs are fundamentally limited by the fraction of the solar spectrum that they absorb (Q_A from [6], equation 1.1.1). One of the desirable characteristics of Lumogen Red 305 is that its absorption spectrum extends into the blue, with a "secondary" absorption peak around 440 nm. This, coupled with its high quantum yield, good stability, and commercial availability, are what make it attractive as an LSC material. At sufficient optical densities, LR305 is capable of absorbing 25% or more of the air mass 1.5 power spectrum, with >95% absorption across the visible range below 600 nm.

With only Lumogen Red 305, however, achieving high absorption in the blue comes at the cost of greatly increased self absorption. For example, 90% absorption at the 440 nm peak also means ~75% absorption at 604 nm - the peak of the molecular emission spectrum. Extrapolating the measured absorbance spectrum of LR305 to 575 nm (peak) optical densities of between 0.5 and 4 and converting to transmission, the effect on self absorption is immediately notable when compared to LR305's molecular emission spectrum (figure 3.2.1).

As the transmission spectrum of LR305 approaches zero across its absorption range, progressively less of the air mass 1.5 power spectrum is absorbed for a fixed percentage optical density increase (figures 3.2.1, 3.2.2). For example, a sample with an absorbance peak of 0.1 will absorb ~ 2.9% of AM1.5 power. Doubling the optical density for a peak absorbance of 0.2 captures 5.5% - 90% increase, but a doubling

optical densities from 2 to 4 absorbance units provides a much more modest 20% gain. The trend may be useful to visualize: figure 3.2.2 plots the percent of AM1.5 power absorbed versus peak optical density for an LR305 PMMA film, using the air mass 1.5 reference solar spectral irradiance published by the National Renewable Energy Laboratory. The gains above a peak optical density of one come mostly from increased absorption in the blue, but at the expense of simultaneously raising the film's self absorption, which continues to grow with optical density as the absorption spectrum saturates in the blue and progressively less solar power is absorbed for a given increase of optical density. With the addition of DCM, high blue absorption - and enhanced LR305 emission from such excitation - can be achieved without altering the film's transmission appreciably at 604 nm - and making films at concentrations where FRET has been shown to be dominant eliminates the additional reabsorption and reemission losses associated with radiative dye transfer and self absorption of the shorter wavelength dye. As a consequence of FRET, one is able to fully saturate the short wavelength dye's absorption without altering that of the emissive dye. In the context of two example films, 0.75% LR305 and 0.5% DCM dye:PMMA ratio by weight, each absorbs 4.9% and 5.8% of AM1.5 power, respectively, with the blended film absorbing 11.15% of the power of the AM1.5 spectrum. Absorbing the same power from LR305 alone would require tripling its peak optical density, an effect which will carry forward to the portion of its absorbance overlapping the emission and drastically increase its self absorption.

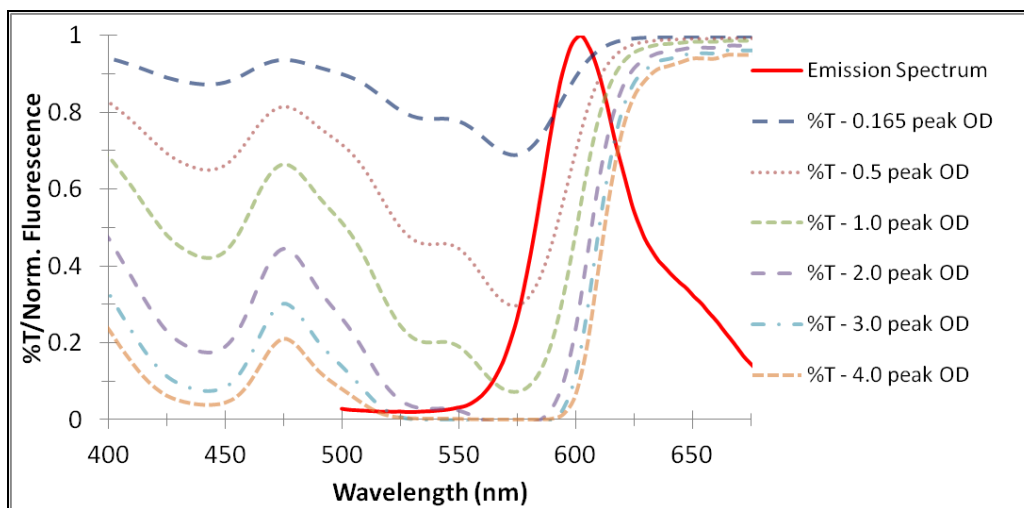


Figure 3.2.1: Increases in the 575 nm (peak) optical density of L305 provide progressively less benefit to AM1.5 absorption, at the expense of greatly increased self-absorption of emitted light. Transmission at given peak optical density is plotted against LR305's own emission to highlight the increase in self-absorption in high optical density LR305 films.

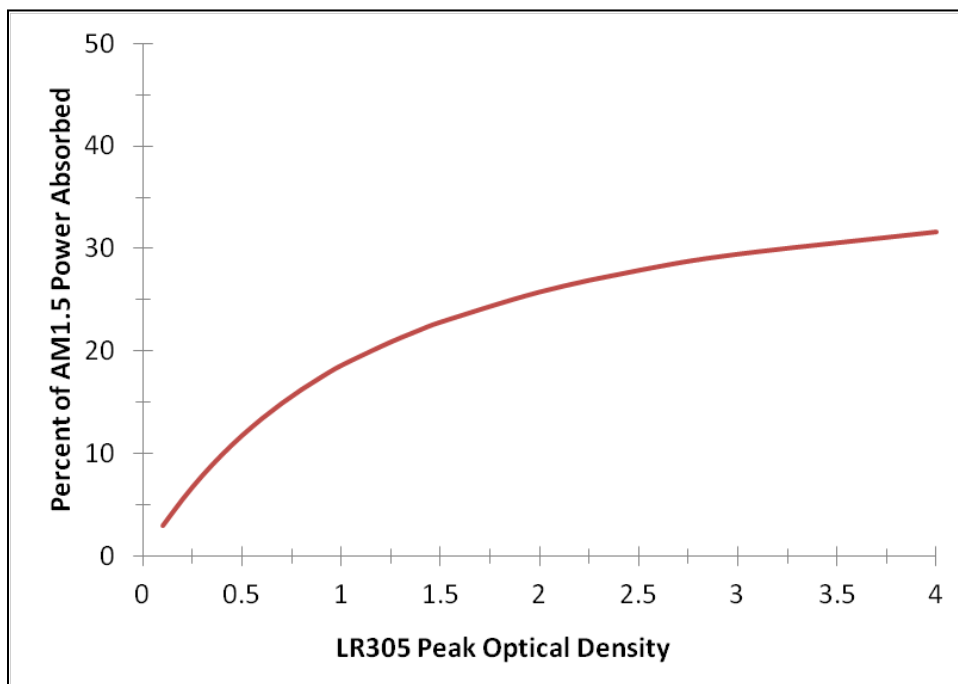


Figure 3.2.2: Percentage of AM1.5 Intensity spectrum absorbed by an LR305 film as a function of its peak optical density. Higher optical density films continue to increase self absorption with progressively less solar photon flux absorption.

A simple way to see an effect of this that is directly related to LSC performance is by examining the inner filter effect [70],[71] as the concentration of the film is increased at the two tested LR305:DCM ratios and compared against pure LR305. At very low optical densities, fluorescence intensity can be expected to be proportional to absorbance. However, above optical densities of about 0.1 at the excitation and/or emission wavelengths, fluorescence intensity begins to deviate - see, for example figure 3 in [71] or [23]. Figure 3.2.3 shows the peak fluorescence intensities observed with doctor-bladed films when excited at 460 nm. The blend with the larger amount of DCM shows a higher fluorescence peak intensity since the emissive side of the inner filter effect is lower for a given 460 nm optical density. Likewise, this peak is achieved at a lower concentration of both total dye and LR305 - resulting in lower self absorption. While these ratios have not been optimized against a particular LSC panel geometry and total AM1.5 absorption, it illustrates the advantage that FRET may provide LSC films in considering future work.

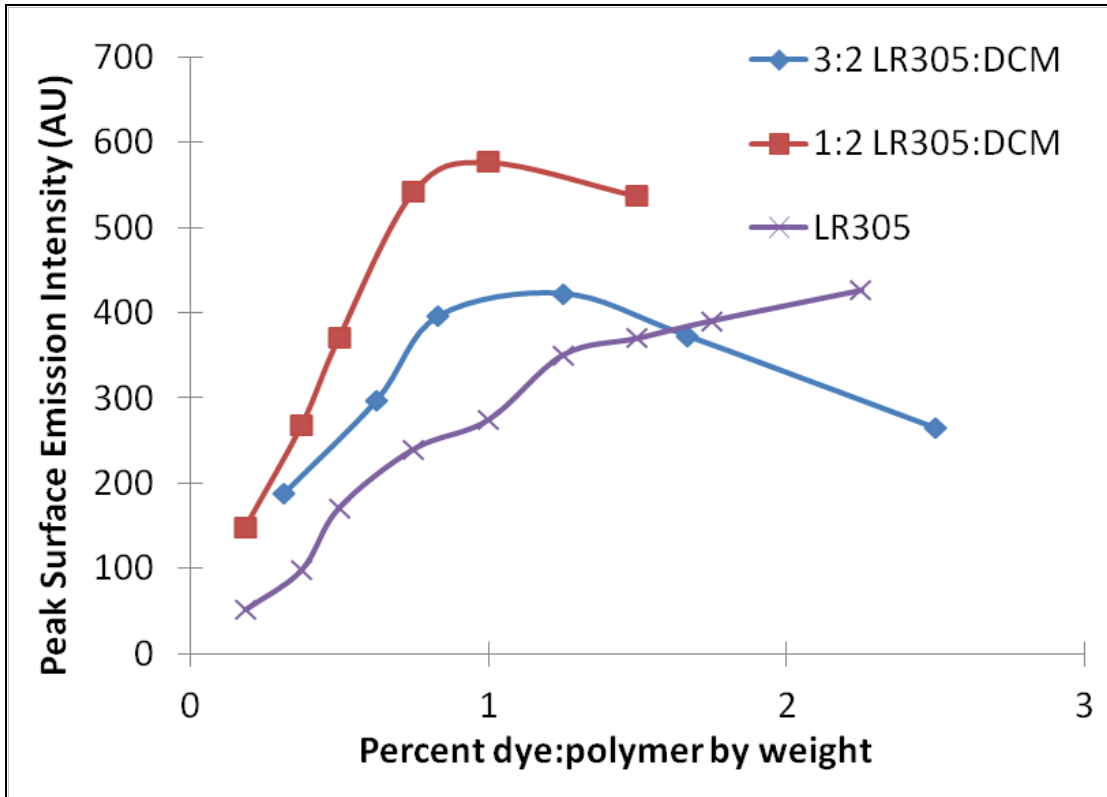


Figure 3.2.3: Comparison of the peak fluorescence intensity of DCM blended and LR305 only films in different ratios as the concentration is varied. Lower acceptor:donor ratios allow for less self absorption of emitted light, reducing the inner filter effect and facilitating brighter surface fluorescence.

3.3 The effect of FRET on waveguide transport losses

When all dyes involved in a planar luminescent solar concentrator have similar quantum yields, as in the case with the two dyes presented in this study, Förster Resonance Energy Transfer is expected to be most useful for reducing waveguide transport losses through reduced absorption and emission events. This serves to reduce both quantum yield losses from each re-absorption as well as the reduction of escape cone losses that result from isotropic re-emission of photons which were

initially trapped within the waveguide. In the interest of experimentally quantifying the benefit provided by FRET to waveguide transport losses (Q_C from eq. 1.1.1), LSC sample devices were prepared as described in section 2.2.

Several experimental issues prevented the use of the intended dyes: DCM and LR305. DCM was found to diffuse from the polymer as the samples were heated in the press. Temperatures of over 150 degrees Celsius were required to melt the 350K molecular weight PMMA obtained for the experiment, resulting in changes to the spectroscopic properties of both dyes. Substitution of Ethylene vinyl acetate (EVA), which has a lower melting point of 80 degrees Celsius, for PMMA showed various solvatochromatic changes to DCM: both red-shifted emission and severely reduced quantum yield, potentially owing to the greater polarity of the new host environment. The replacement dyes obtained, hereafter referred to as the "short" and "long" wavelength dyes based on their relative emission and absorption spectra, are of proprietary formulation but have been shown to be of similarly high quantum yield in EVA (discussed below) and photostable throughout the length of the experiment.

Quantum-yield measurements were taken with a Hamamatsu Quantaurus absolute PL quantum yield spectrometer with appropriately tuned monochromatic excitation across the absorption range of both dyes. The spectrometer is a self-contained unit which uses an integrating sphere and xenon arc lamp to measure quantum yield by comparing energy-adjusted excitation and emission intensities against a reference:

$$\phi_F = \frac{\text{PhotonEmission}}{\text{PhotonAbsorption}} = \frac{\int \frac{\lambda}{hc} [I_{\text{emission}}^{\text{sample}}(\lambda) - I_{\text{emission}}^{\text{reference}}(\lambda)]}{\int \frac{\lambda}{hc} [I_{\text{excitation}}^{\text{sample}}(\lambda) - I_{\text{excitation}}^{\text{reference}}(\lambda)]} \quad (3.3.1)$$

the system has been used in many published works such as [72]. The results, with excitation swept across the absorption spectra of each of the fluorophores, shows measured quantum yields between 0.85 and 0.925 as plotted in figure 3.3.1. The excitation and emission spectra of the "short" and "long" wavelength dyes, in turn, are shown in figure 3.3.2.

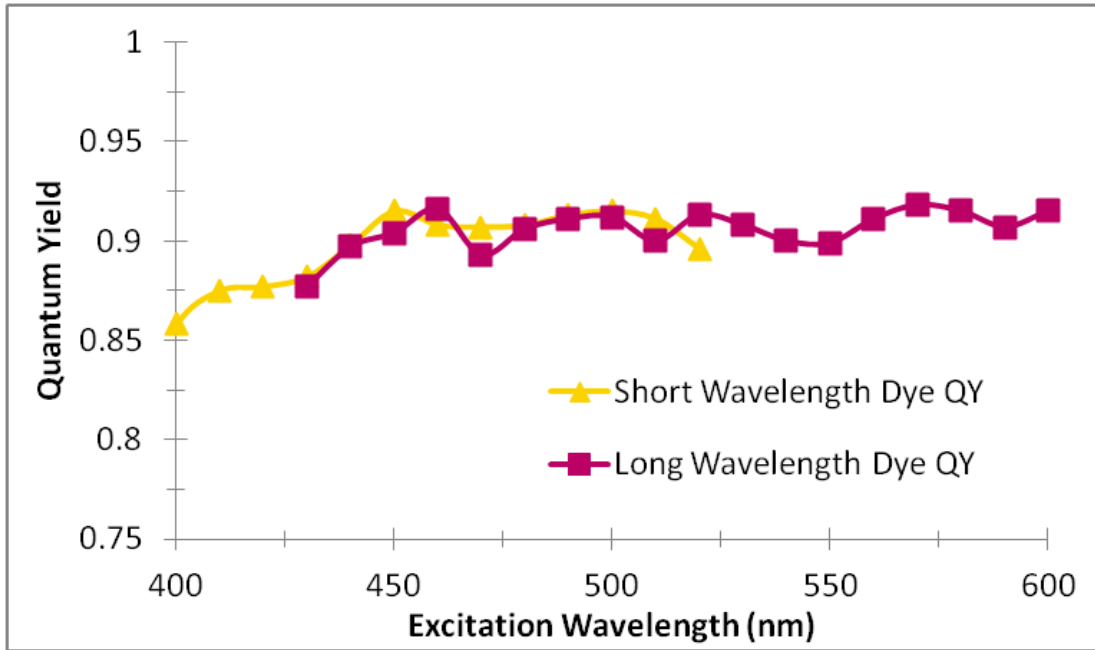


Figure 3.3.1: Excitation wavelength dependent quantum yield measurements of the short and long wavelength dyes in EVA, as measured by Hamamatsu PL QY spectrometer.

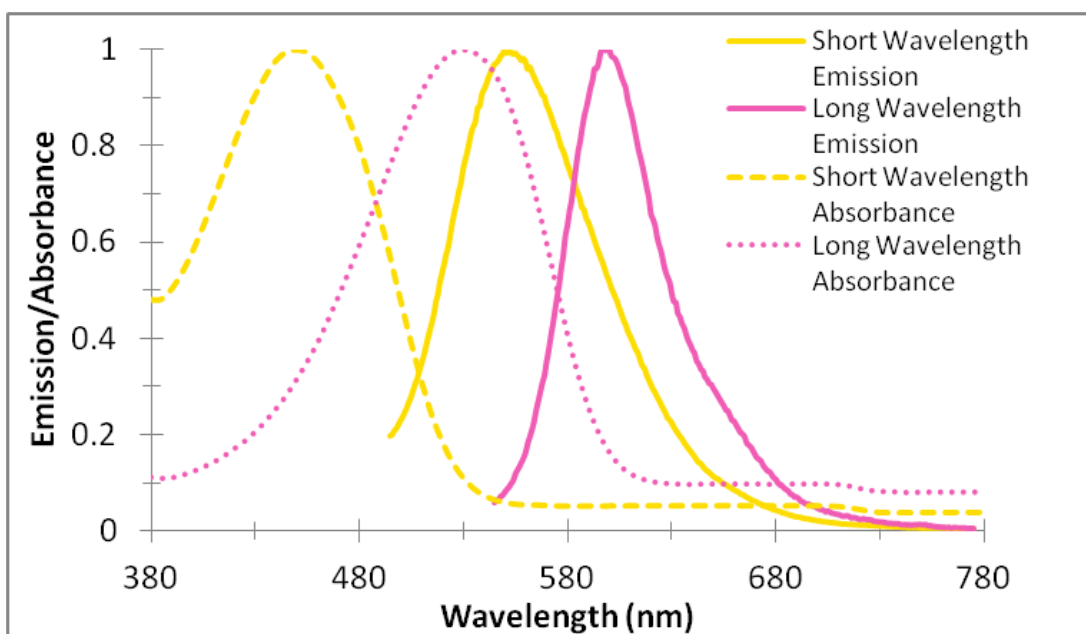


Figure 3.3.2: Emission and absorbance spectra of the short and long wavelength dyes used in this section. Emission spectra taken with excitation at respective peak absorbance wavelengths.

The broader spectral overlap of the short wavelength dye emission and long wavelength dye absorption when compared to that of DCM and LR305 in PMMA give a larger calculated critical Förster distance (R_0); from spectroscopic data the distance at which nonradiative energy transfer is estimated to be 50% efficient was calculated to be 53.4Å. Using equation 3.1.2 we then see that the probability of FRET increases significantly when the average donor-acceptor pair distance is less than this (figure 3.3.3). Comparing this efficiency with the concentration regimes estimated from the LR305:DCM in PMMA system, this is estimated to be in range of 0.2% total dye:host polymer by weight.

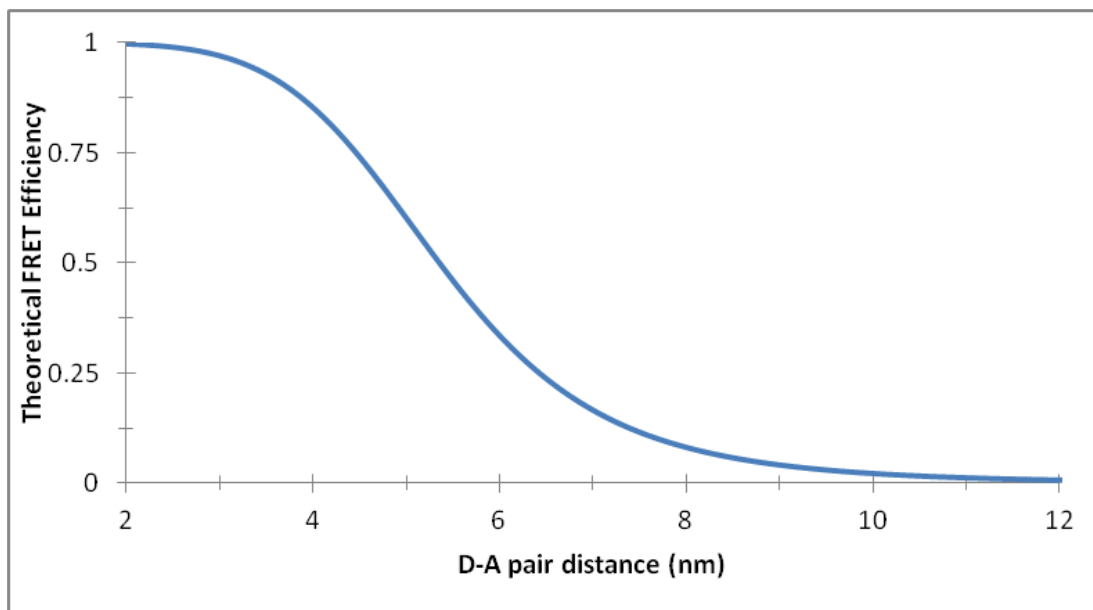


Figure 3.3.3: Calculated FRET efficiency as a function of D-A pair separation for short and long wavelength dyes used in this experiment.

The edge emission spectra of both the "low density" and "high density" samples (described in section 2.2) were taken by optically coupling a fiberoptic cable into the edge of the device (with index matching optical gel), and using a 405 nm LED as the excitation source in the center, as shown in figure 3.3.4.

The excitation wavelength was chosen specifically to initially excite the donor fluorophore. Even in the absence of FRET, one would expect to see little donor emission at the edge: the optical density of the acceptor is large over the donor's emission spectrum. This effect is noted in several other papers considering LSC efficiency, such as [20] and [27]. The resulting emission spectra are compared with the "molecular" emission spectrum of an acceptor-only film (figure 3.3.5). The "molecular" emission spectrum was taken from a very thin spin-cast film with an optical density of <0.05 in order to minimize self absorption.

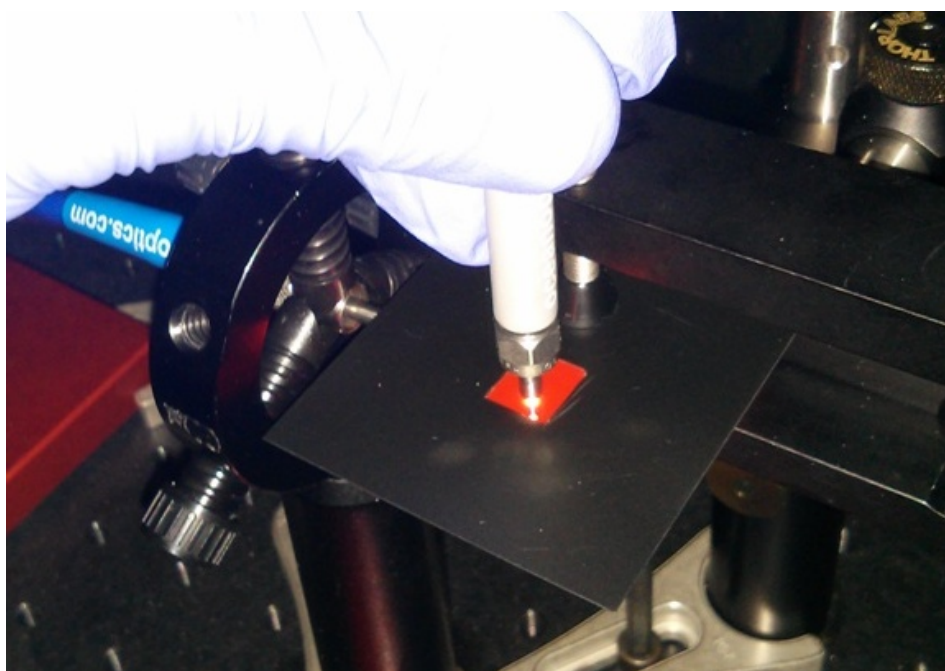


Figure 3.3.4: Experimental determination of LSC sample edge emission under 405 nm excitation.

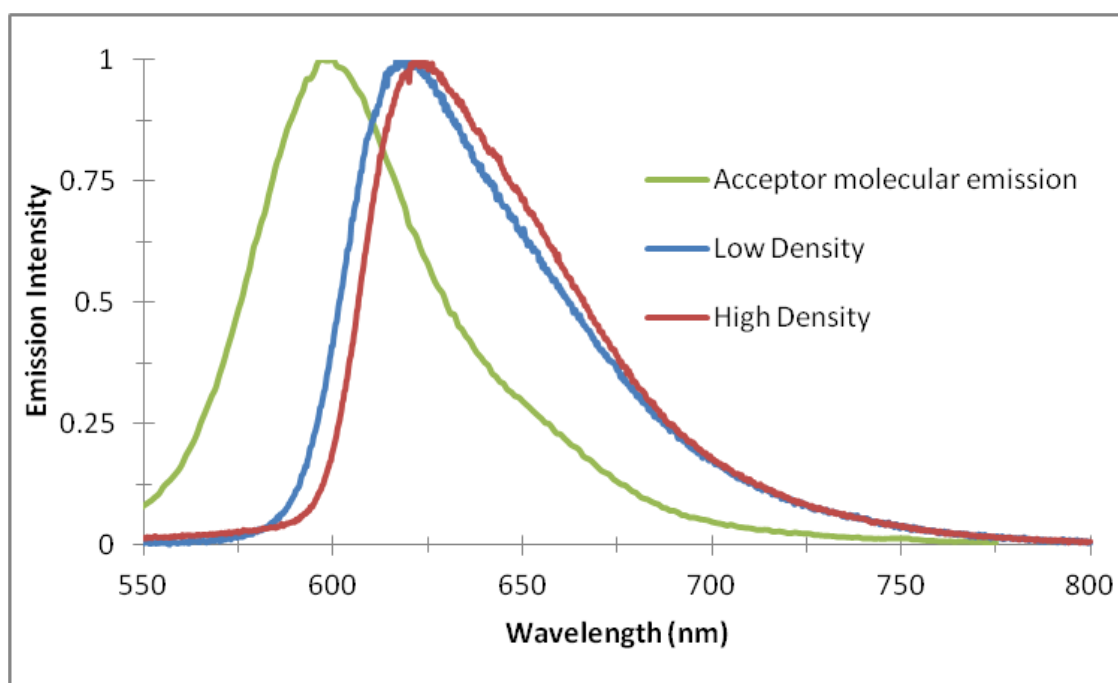


Figure 3.3.5: Comparison of the "low" and "high" concentration LSC sample edge emission with the thin-film emission from an "acceptor" (long wavelength dye) only film.

As can be seen in figure 3.3.5, the edge emission spectra of both the low and high density samples are similarly redshifted from the molecular emission of the acceptor. However, there is a notable difference in the edge emission of the "low" and "high" density films: a 3 nm peak shift (618 nm to 621 nm) is observed. While the difference could be due to a small variation in the optical density of the two samples, FRET may also play a role here: in addition to a small portion of the donor fluorescence reaching the detector and causing a slight blueshift in the peak, a larger fraction of the reabsorption events in the "high density" sample should be from acceptor emission since light absorbed by the donor will be immediately radiated by the acceptor, rather than traveling through some portion of the total optical density before being absorbed by the long wavelength dye.

The ultimate goal of this experiment was to investigate transport losses as a function of excitation wavelength. As described in section 2.2, commercially obtained cSi cells were coupled into the LSC edge with index matching optical adhesive. Prior to attachment the cells were tested with an Oriel IQE 200 quantum efficiency measurement system. The system allows for measurement of incident photon to charge carrier efficiency such that the external quantum efficiency (EQE) is defined as:

$$\eta_{Quantum} = \frac{\eta_{electrons}}{\eta_{photons}} \quad (3.3.2)$$

The cells themselves were found to have typical fill factors and open circuit voltages for commercial-grade crystal silicon: ~70% and 0.6V, respectively. The external

quantum efficiencies of the glass-laminated cell used in the experiment was measured before coupling to the LSC and is shown in figure 3.3.6. where the EQE is seen to be constant over the range of the LSC device edge emission spectra. In order to directly compare transport losses, then, an adjustment scheme was devised to normalize against the dye absorption spectrum and geometric considerations. The Oriel IQE 200 excites with a small area, intensity calibrated beam of $<0.25 \text{ cm}^2$, as can be seen in figure 3.3.7, a photo taken of an actual device in the test setup.

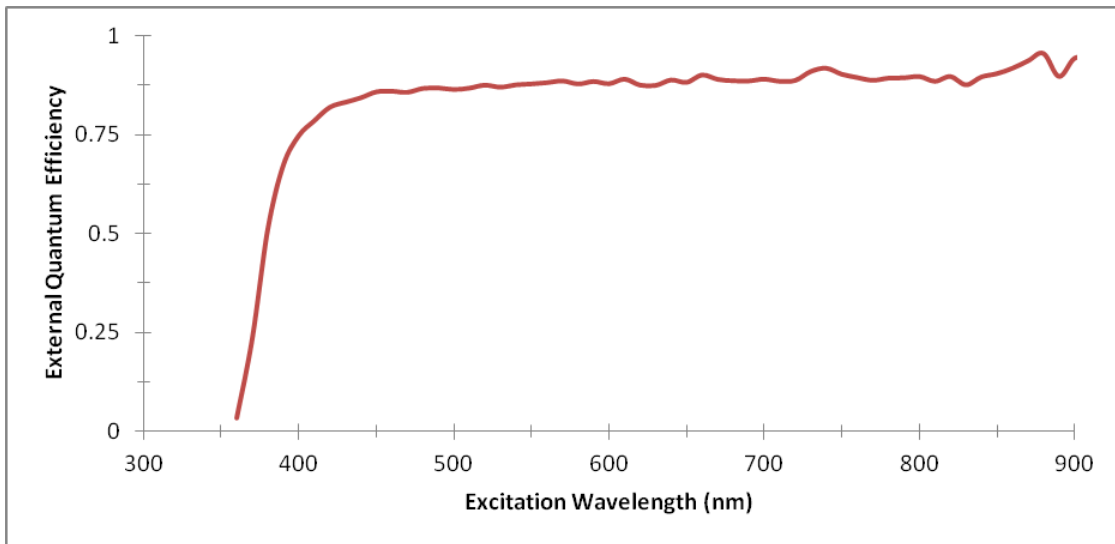


Figure 3.3.6: EQE measurement of a cSi cell used in the experiment. Response is seen to be even across the range of the emission spectrum detected at the LSC edge.

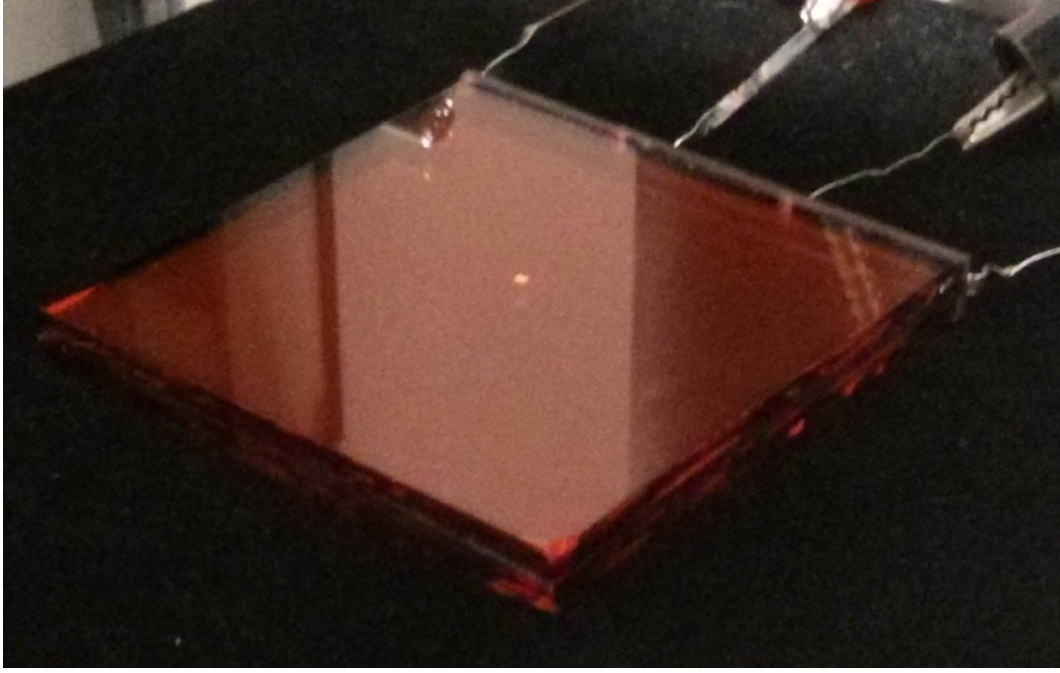


Figure 3.3.7: Sample LSC device with intensity calibrated excitation visible in the device's center.

where the incident beam is notable in the center of the device from Fresnel reflection at the glass-air interface. In this way, EQE was measured in the center cell. For a given excitation wavelength, this value was first normalized against the film's absorption at that wavelength. Then, with the assumption that light would be transported uniformly in all directions from the point of excitation, the fraction of the unit circle subtended by the tested cell is given by the geometric normalization factor defined below as G_{nc} :

$$G_{nc} = \frac{1}{\pi} \tan^{-1}\left(\frac{1}{R_0}\right) \quad (3.3.3)$$

where R_0 is defined as the distance from the center of the solar cell to the point of excitation as shown in figure 3.3.8. An important consideration is that the average horizontal distance between the point of excitation and the solar cell will be greater than R_0 and may be calculated as:

$$R_{eff} = \int_0^1 \sqrt{x^2 + R_0^2} dx \quad (3.3.4)$$

but at distances of more than 1 cm, R_{eff} quickly approaches R_0 such that this factor makes a progressively smaller impact. It was similarly seen that, at distances above approximately 1 cm, after geometric normalization, adjusted EQE did not vary in a way correlatable to excitation distance, as can be seen in averaged "adjusted" EQE data, shown in figure 3.3.9 for the low density film.

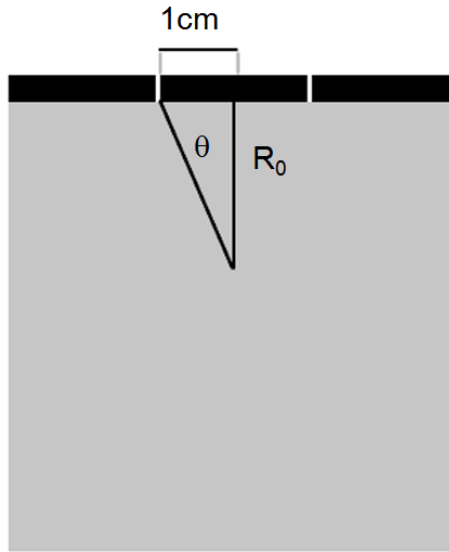


Figure 3.3.8: Schematic showing how R_0 (the distance from the point of excitation to the center of the center cell) is defined to calculate the geometric normalization factor G_{nc} . LSC is viewed from above in this figure.

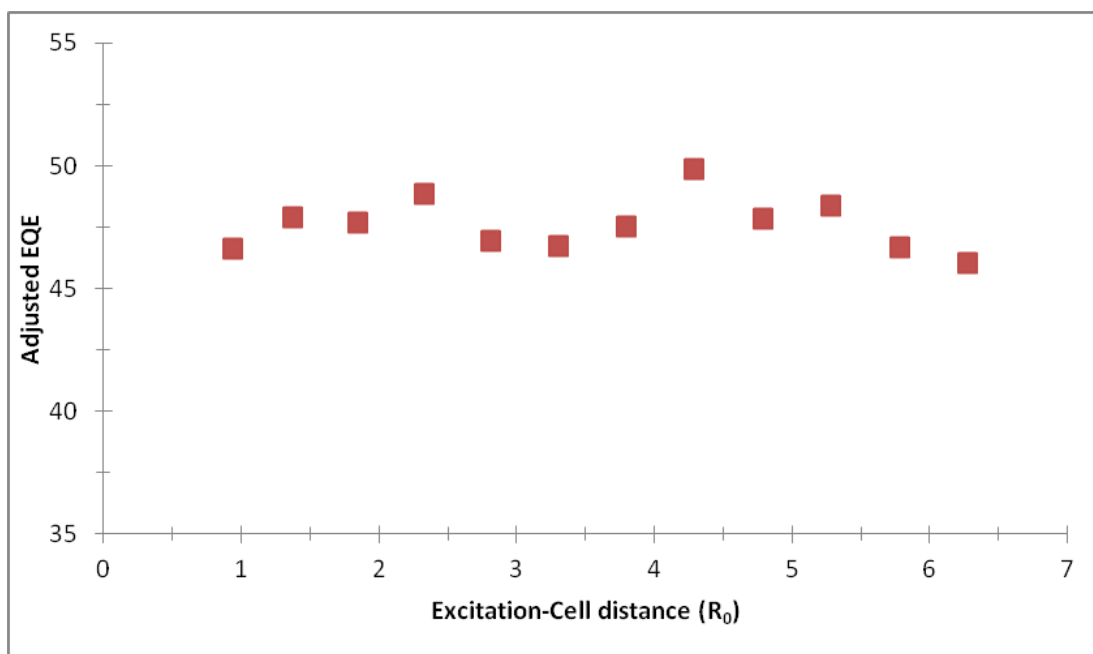


Figure 3.3.9: Average "adjusted" EQE (averaging the wavelength dependent adjusted EQE over the relevant range).

Comparing the edge emission shown in figure 3.3.5 with the absorbance spectra given in figure 3.3.2, it becomes clear that the edge emission detected from excitation in the center will not be subject to appreciable re-absorption. Thus it may be surmised that re-absorption losses happen largely over a distance of less than 1 cm in these films, given the seemingly random variation of average EQE about a mean at larger distances. As such, averaging the adjusted EQE measurements at distances between 1-6 cm will provide additional sample points to reduce random error. A notable trend is thus revealed by averaging the adjusted EQE values at each wavelength across the various excitation distances and comparing the results to the absorbance contribution of the short and long wavelength dyes. The expectation is that FRET should

ultimately benefit the transport efficiency (and thus the "adjusted EQE" defined in this section) of photons absorbed by the short wavelength dye. The results should be refelected in the total transport losses at excitation distances greater than the "self absorption" regime. In the preliminary experiments conducted in the course of this work, a trend to that effect is visible, and is plotted in figure 3.3.10. While the "high density" LSC sample in which FRET is expected to play a larger role has a relatively flat transport loss across its absorption range, the "low density" sample shows a transport loss which decreases as a larger fraction of the incident photons are absorbed by the long wavelength dye directly, and approaches that of the "high density" sample as the short wavelength dye's contribution to the total absorption approaches zero. While it can be readily shown that multiple dyes will increase overall LSC efficiency by absorbing more of AM1.5 power [21], and as discussed in section 3.2, a working experimental demonstration of actual benefits FRET affords transport losses over trivial re-absorption is presented here for future criticism or reproduction.

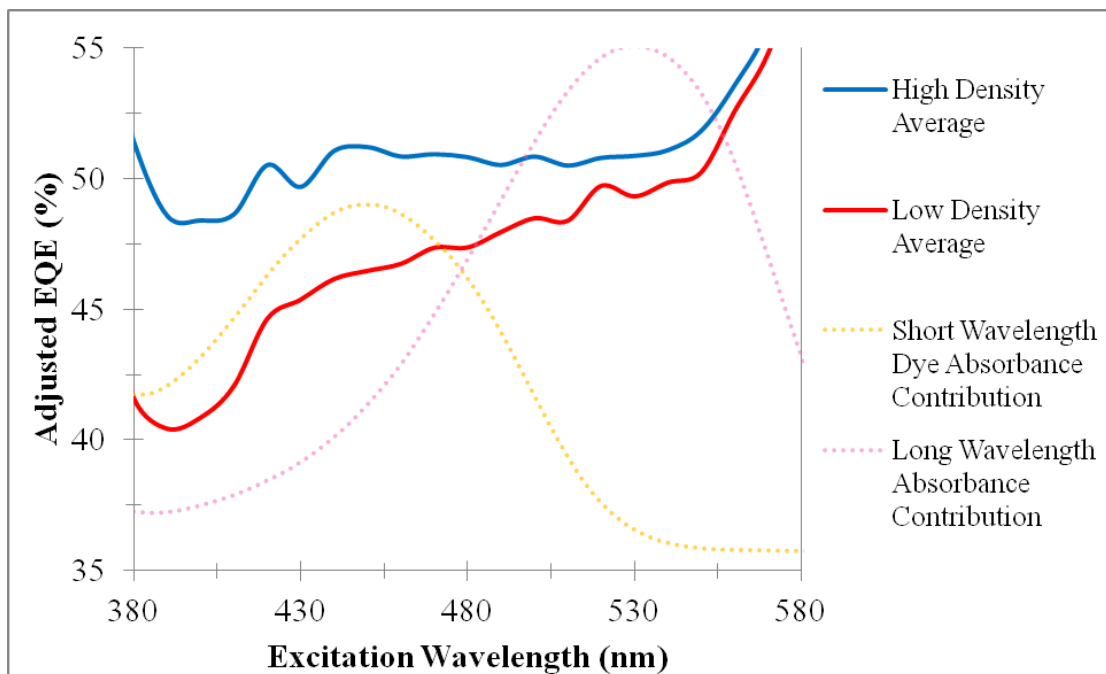


Figure 3.3.10: Comparison of transport efficiency between the "low" and "high" density LSC samples as a function of excitation wavelength. Absorbance spectra of short and long wavelength dyes are shown for comparison. Note that the adjusted EQE normalizes against absorption of each film.

Chapter 4

4.1 The role of FRET, fluorescence spectrum on film color

Another advantage owed to efficient transfer between multiple dyes in the LSC film is color tunability. Perceived color of the film is determined almost solely by the transmitted light, and fluorescence is shown to have very little impact on measured transmission. Comparing the transmission spectra of a 0.16 peak optical density LR305 film from the thin film measurement system with that taken in a dual-monochromometer absorbance spectrometer, it is seen that there is little perceivable difference in the measured transmission of the film (figure 4.1.1):

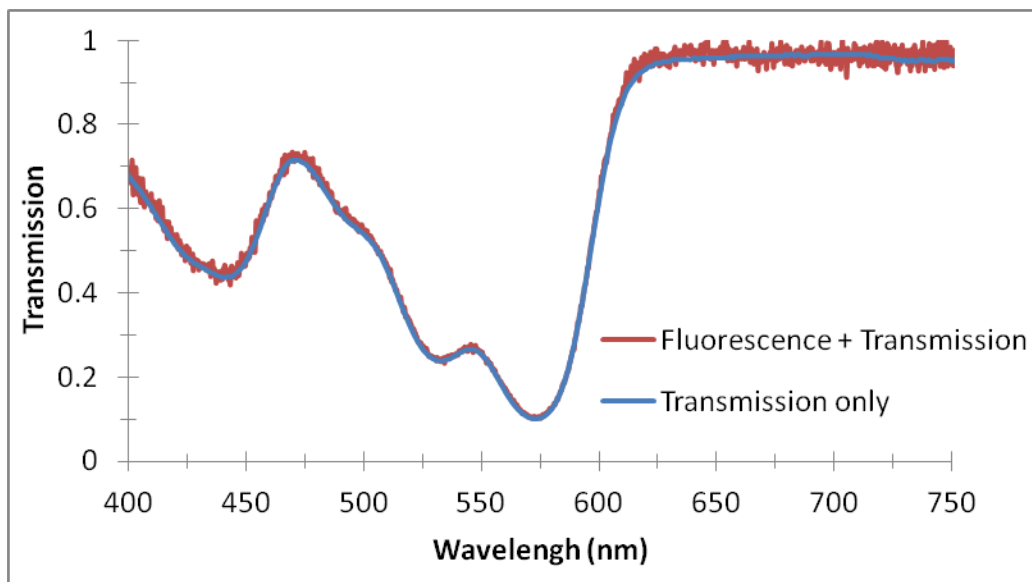


Figure 4.1.1: Comparison of transmitted light both with (thin film measurement system) and without (dual-monochromometer UV-Vis spectrometer) fluorescence intensity included.

While the former setup uses a simulated white "reference" lightsource with appropriate background subtraction and should collect transmission and fluorescence

of the film, the latter will minimize detected fluorescence as transmission at any given wavelength is measured under a narrow bandwidth excitation rather than a white "reference" spectrum. Were film fluorescence to have a measurable impact, one would expect to see the fluorescence of the Lumogen dye above the transmission baseline in the thin film system measurement between 600 and 650 nm; any gain is not discernible from the noise floor of the measurement.

The acceptance cone of the optical fiber used in the thin film measurement system may reduce the measured impact of fluorescence on transmission; while an area surface element of the film will fluoresce into its escape cone, the acceptance cone of the optical fiber is likely smaller [27]. However, a real observer at a distance from the LSC material would also observe limited fluorescence angles from a fixed area element of the film.

It is not surprising that fluorescence is seen to have little impact on the measured transmission; the top escape cone for any fluorescent volume element covers just under 13% its total solid angle (see equation 1.1.3). Additionally, any impact on the transmission spectrum is determined by the ratio of the film's fluorescence intensity at a given wavelength to the incident light source intensity at that wavelength. At low optical densities, very little light is absorbed. At higher optical densities, the inner filter effect will further limit the detectable fluorescence intensity, in addition to the geometric limitations.

Thus one can reasonably argue that while fluorescence cannot generally be neglected in determining color [31, section 3.7], in the case of planar LSC films we

can consider only absorption, and film color tunability is calculable from the additive absorbance of multiple dyes. The addition of DCM shifts the pink-red range of LR305 films towards orange, however using as few as three appropriately absorbing dyes (discussed further in section 4.2), a large portion of the visible spectrum may be covered. Film color can be predicted according to a subtractive scheme such as the CMY color model. As can be seen in figure 4.1.2, the various color possibilities achievable are shown, in a CIE1931 xy chromaticity diagram with data taken from the thin film measurement system. The figure includes data from the single LR305 dyes, the blended LR305 and DCM dye films, LR305 with a red absorber (LD700

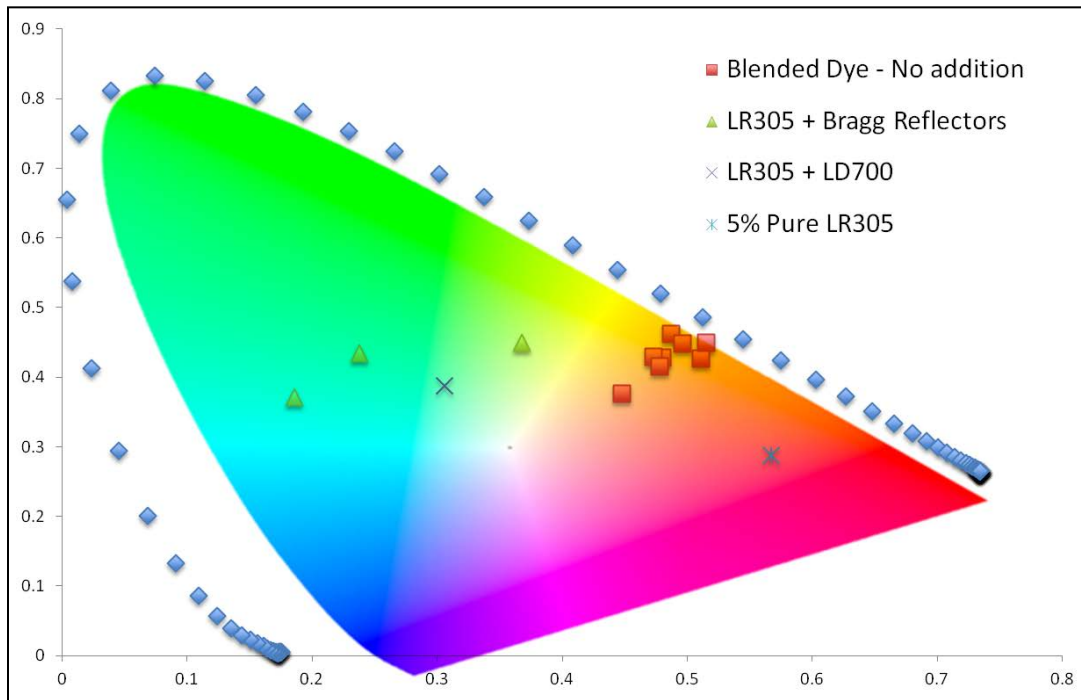


Figure 4.1.2: Various color possibilities are plotted on a CIE 1931 xy chromaticity diagram. Data are taken from samples measured with the thin film measurement system described in section 2.1. CIE 1931 xy chromaticity may be derived from CIE XYZ colorspace values from a suitable transformation.

Perchlorate, excitation chemical co.), and LR305 with a dielectric bragg reflector placed in front of the film at various angles to simulate different absorbance spectra. Efficient FRET becomes increasingly important as more dyes are used in order to minimize waveguide efficiency losses.

4.2 LSC color calculation from a subtractive CMY color model

Noting that LSC color, as seen by an observer for whom edge emission is not visible, is determined primarily by the absorption spectrum of the LSC layer, it is possible to use the Beer-Lambert law to predict LSC color as well as optimize a particular set of fluorophores for a desired result. As an example, a method is presented to demonstrate how relative dye concentrations in a multiple-dye setup may be adjusted to achieve a 'neutral' color. Through a conversion to the appropriate colorspace and neglecting aggregation effects of dyes as a function of concentration (that is, assuming absorbances vary linearly with the optical density of a given fluorophore), determination of the appropriate concentration ratios for the multiple dyes can be reduced to a simple optimization problem.

Since perceived color will be determined predominantly by the transmission of the incident light which reaches the observer, it is easiest to begin by considering a reference white spectrum, such as a D65 lightsource whose intensity profile is shown in figure 4.2.1.

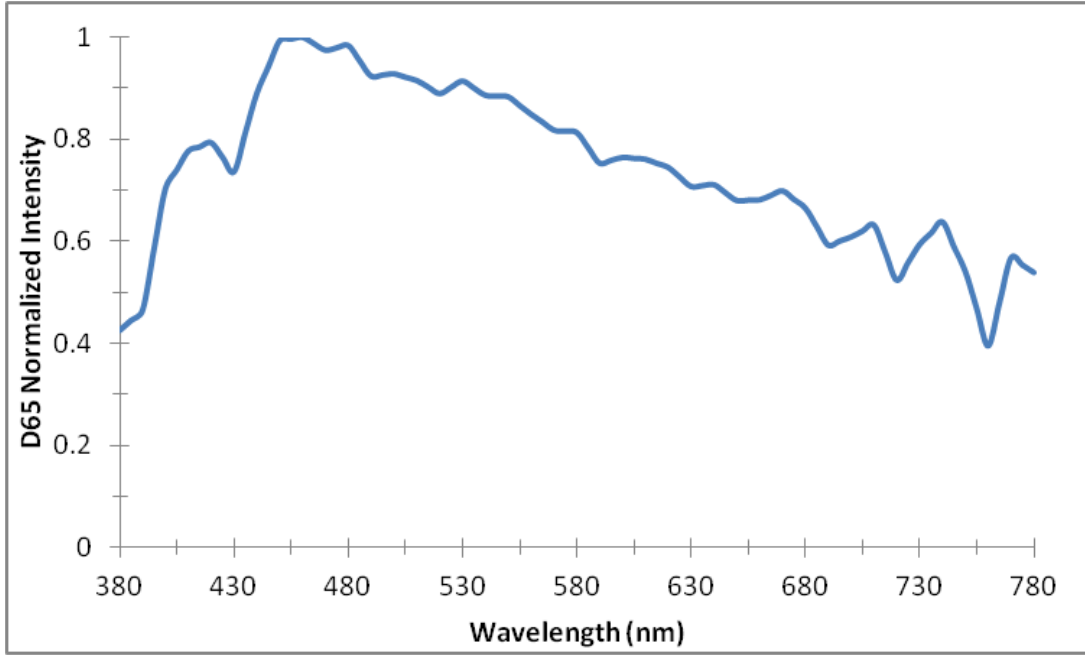


Figure 4.2.1: A normalized sample D65 spectrum

The total absorbance of the film at an incident wavelength $A_{TOT}(\lambda)$ can then be defined as:

$$A_{TOT}(\lambda) = l(\varepsilon_1(\lambda)c_1 + \varepsilon_2(\lambda)c_2 + \dots + \varepsilon_n(\lambda)c_n) \quad (4.2.1)$$

where ' l ' represents the optical pathlength of the sample (which in the case of an observer viewing the film at normal incidence is simply its thickness), and $\varepsilon_n(\lambda)c_n$ represent the wavelength dependent absorbance coefficient and concentration of the n^{th} absorbing sample, respectively. As can be seen from the Beer-Lambert law, $A_{TOT}(\lambda)$ varies linearly with the concentration of each absorbing species. Noting that the intensity of a reference lightsource which reaches an observer will be governed according to wavelength dependent transmission, it is seen from the Beer-Lambert law that:

$$I_T(\lambda) = I_{0-D65} \cdot \%T = I_{0-D65} \cdot 10^{-A_{TOT}(\lambda)} \quad (4.2.2)$$

where I_T is the transmitted intensity at a given wavelength, and I_{0-D65} is the intensity of the reference lightsource, here presented as a D65 white reference. $A_{TOT}(\lambda)$ is related to the transmitted intensity by:

$$A_{TOT} = \log \left(\frac{I_{0-D65}}{I_T} \right) \quad (4.2.3)$$

such that the intensity profile which reaches an observer's eye from a mixture of n absorbing species can be reduced to a function $I_T(\lambda, c_1, c_2, \dots, c_n)$ and constant values since, absent aggregation effects at high concentrations in some fluorophore species, absorbance spectra do not generally change shape as optical density is varied.

It is this spectral power distribution derived from equation 4.2.2 that determines perceived color, and can be used to represent the color of the film as perceived by an observer in many difference color spaces. As an example, the conversion of the transmitted spectral power to one of the two first mathematically defined colorspace, the CIE 1931 XYZ colorspace is presented. The CIE 1931 XYZ colorspace was established in the indicated year by Commission internationale de l'Eclairage ("International Commission on Illumination," or CIE) as the color viewed by a human observer according to the spectral response of three types of color receptors in the eye. While the history of the development of relating spectral power distribution to perceived color is outside the scope of the work presented here, a

detailed description is available in many texts such as [73] and [74]. In the case of the CIE 1931 XYZ colorspace, color is represented by three 'tristimulus' values X,Y,Z, which are determined by multiplying the spectral power distribution by appropriate receptor-specific wavelength dependent weighting functions and integrating over the visible range of wavelengths such that X, Y, and Z are given by [74]:

$$\begin{aligned}
 X &= \int_{380nm}^{780nm} I_T(\lambda) \bar{x}(\lambda) d\lambda \\
 Y &= \int_{380nm}^{780nm} I_T(\lambda) \bar{y}(\lambda) d\lambda \\
 Z &= \int_{380nm}^{780nm} I_T(\lambda) \bar{z}(\lambda) d\lambda
 \end{aligned} \tag{4.2.4}$$

with the wavelength dependent weighting ("color-matching") functions \bar{x} , \bar{y} , and \bar{z} given as in figure 4.2.2 for a CIE 1931 XYZ colorspace. Note that while the CIE 1931 xy chromaticity values plotted in figure 4.2.1 may be derived from CIE XYZ values through a suitable transformation, the X,Y and x,y values are distinct.

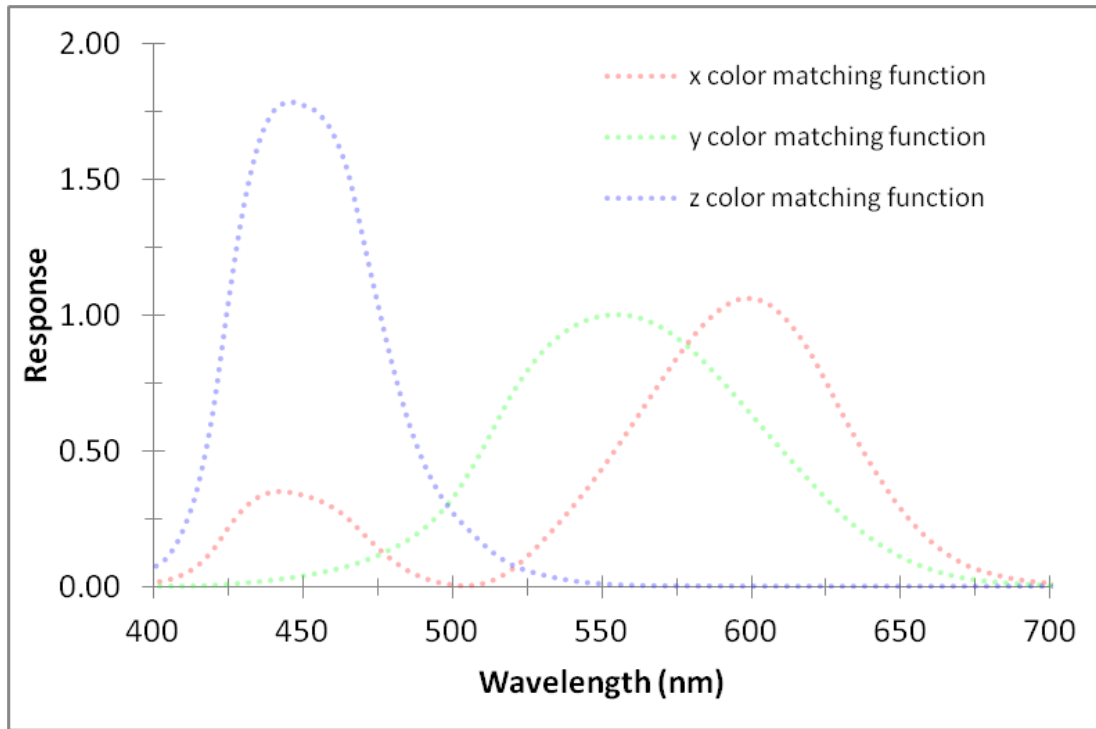


Figure 4.2.2: CIE XYZ color matching functions used to determine CIE XYZ values. Color matching functions are determined largely from the spectral response of human color receptors.

Thus, a method is established which allows one to numerically construct a space depicting possible color combinations of an LSC with n absorbing species. Given a fixed LSC thickness, and known absorbance coefficients of all the absorbers involved, any point in this space may be defined in terms of the concentration of each absorber allowing one to predict the necessary concentrations to achieve a desired color.

As an example application, one may consider the CMY (cyan, magenta, yellow) "subtractive" color model. In contrast to the commonly used RGB "additive" color model, in which black is considered the absence of color and red, green, and

blue "primary" colors are added to produce the desired spectral intensity profile, a white reference spectrum is considered the absence of color, and color is determined by what is subtracted from that reference, as is the case when considering absorbing species in an LSC-type host polymer. Subtractive color models are commonly used in printing, where inks are deposited according to what they will absorb from a white reflector (for example, paper). Absorbers which will individually correspond to transmitted intensities perceived by an observer as cyan, magenta, and yellow when their absorbance is subtracted from a "white" lightsource (the D65 lightsource, for example, shown in figure 4.2.3), form the primary colors for a "subtractive" color scheme:

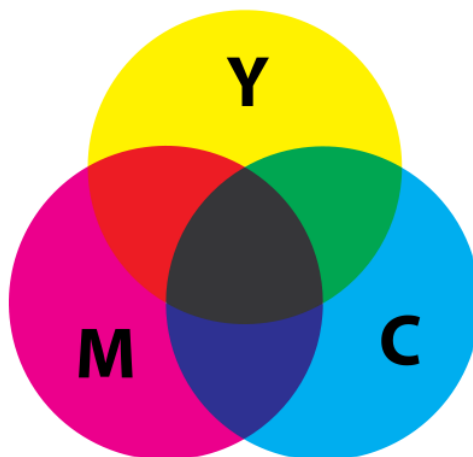


Figure 4.2.3: Overlay of primary subtractive colors: cyan, magenta, and yellow absorbers may be combined to cover a large portion of the visible spectrum.

Thus, with as few as three appropriately absorbing fluorophores, a large portion of perceivable colors may be represented by adjusting the various concentration ratios. In order to provide an example application for the method, one may consider the

absorbance spectra of the "short" and "long" wavelength proprietary formulated dyes used in section 3.3 of this work, now referred to as "yellow" and "magenta" absorbers, respectively. With the addition of a "cyan" fluorescent absorber, also of proprietary structure (normalized absorbance spectra shown below in figure 4.2.4) we now have the ingredients necessary to determine calculate a large portion of the visible spectrum as a function of the concentrations of the three absorbers. It is useful to note that the colors associated with the "primary" absorbers in figure 4.2.4 are represented by their appearances: for example, while the "cyan" absorber has its absorption peak in the red, it will appear cyan when its absorption is subtracted from a white reference and the transmitted spectrum is weighted against the color response

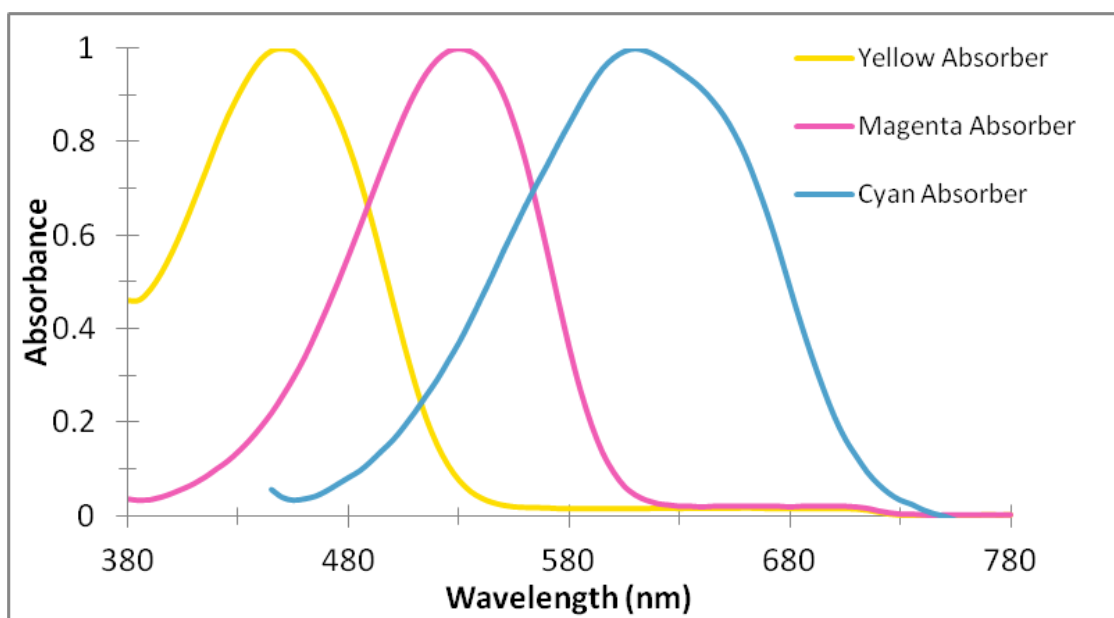


Figure 4.2.4: Absorbance spectra of approximate "primary color" absorbers. Note that the absorption spectra are coded according to how they appear when their absorption is subtracted from a white light source - while the "cyan" absorber has an absorption peak in the red, it has higher transmission in the blue, thus its perceived color, one weighted against the spectral response of human color receptors (see figure 4.2.2).

of a human observer.

As an example application, as mentioned at the beginning of this section, it is possible to determine the ratio of absorbers needed to achieve a "neutral" or gray color through a numerical optimization process. Consider the *CIE 1976 $L^*a^*b^*$* colorspace, definable through the following transformations from CIE 1931 XYZ values (equations 4.2.4) as given in [74]:

$$\begin{aligned}
 L^* &= 116f\left(\frac{Y}{Y_n}\right) - 16 \\
 a^* &= 500\left[f\left(\frac{X}{X_n}\right) - f\left(\frac{Y}{Y_n}\right)\right] \\
 b^* &= 200\left[f\left(\frac{Y}{Y_n}\right) - f\left(\frac{Z}{Z_n}\right)\right]
 \end{aligned} \tag{4.2.5}$$

with X_n, Y_n, Z_n denoting the CIE 1931 XYZ values of the reference lightsource, and the function $f(x)$ given by:

$$f(x) = \begin{cases} x^{1/3} & x > \left(\frac{6}{29}\right)^3 \\ \frac{1}{3}\left(\frac{29}{6}\right)^2 x + \frac{4}{29} & \text{otherwise} \end{cases} \tag{4.2.6}$$

The purpose of using *CIE 1976 L* a* b** colorspace for this example is straightforward: in an "L-a-b" - type colorspace, the *a* and *b* values represent color on a red-green and blue-yellow scale, respectively, and the *L* coordinate represents the "brightness" of the color. Taking 2 dimensional cross sections of the colorspace, an (*a**, *b**) coordinate of (0,0) represents a "neutral" color, with an associated *L* value of 0 representing black, 100 representing white, and everything in between various shades of gray. Thus, to achieve a neutral color, the problem is reduced to the minimization of a single variable which may be defined as:

$$\Gamma = \sqrt{(a^*)^2 + (b^*)^2}$$

Γ may now be defined in terms of the concentrations of the various absorbers: $\Gamma(c_1, c_2, \dots, c_n)$ such that for an arbitrary combination of fluorescent LSC dyes with known absorbances, " Γ -space" may be generated numerically for a distribution of possible concentrations and a minima found such that the "most neutral" color is achieved for the included chromophores.

Chapter 5

Conclusions

This research was oriented towards the goal of increasing single-layer Luminescent Solar Concentrator (LSC) efficiency. An absorption cross section between two LSC dyes, LR305 and DCM, was observed to be larger than expected

from trivial emission and re-absorption in a PMMA host. Förster Resonance Energy Transfer (FRET) is proposed to explain the efficient nonradiative transfer of excitation from the DCM to LR305 dye. An illustration of how this might be exploited to increase AM1.5 power absorption of a given film without altering self absorption is provided. "High density" and "low density" sample LSC devices with coupled PV and the same optical densities were fabricated and a difference in efficiency was detected when the short wavelength dye was responsible for a larger portion of the total film absorption. Efficiencies were shown to approach similar values at longer wavelengths where the short wavelength dye did not absorb incident radiation, suggesting that the difference in transfer mechanisms was responsible for the improvement. The impact of LSC film fluorescence on perceived film color is shown to be minimal, with color largely determined by the absorption spectrum of the film. While FRET will not impact the absorption spectrum, it will improve transfer efficiency between multiple absorbers and therefore plays a role in LSC color tunability: concentrations high enough to exploit FRET in a given LSC setup should be established.

References

- [1] C. Corrado, S.W. Leow, M. Osborn, E. Chan, B. Balaban, S.A. Carter, " Optimization of power gain and energy conversion efficiency using front-facing photovoltaic cell luminescent solar concentrator design," *Solar Energy Materials and Solar Cells* Vol. 111, 74-81 (2013).
- [2] G. Keil, "Radiance Amplification by a Fluorescence Radiation Converter," *Journal of Applied Physics*, Vol. 40, No. 9, 3544-3547 (1969).
- [3] W.A. Shurcliff, "Radiance Amplification by a Multi-Stage Fluorescence System," *Journal of the Optical Society of America*, Vol. 41, No. 3, p209 (1951).
- [4] R.L. Garwin, "The Collection of Light from Scintillation Counters," *Review of Scientific Instruments*, Vol. 31, p 1010 (1960).
- [5] G. Seybold, G. Wagenblast, "New perylene and violanthrone dyestuffs for fluorescent collectors," *Dyes and Pigments*, Vol. 11, Issue 4 (1989).
- [6] W.H. Weber, J. Lambe, "Luminescent greenhouse collector for solar radiation," *Applied Optics* Vol. 15, No. 10, 2299-2300 (1976).
- [7] A.M. Hermann, "Luminescent solar concentrators - a review," *Solar Energy*, Vol. 29, No. 4, 323-329 (1982).
- [8] M.G. Debijs, P. Verbunt "Thirty Years of Luminescent Solar Concentrator Research: Solar Energy for the Built Environment," *Advanced Energy Materials*, Vol. 2 Iss. 1, 12-35 (2012).
- [9] J.S. Batchelder, A.H. Zewail, T. Cole, "Luminescent solar concentrators. 1: Theory of operation and techniques for performance evaluation," *Applied Optics*, Vol. 18, Issue 18, p3090-3110 (1979).
- [10] J. S. Kang, G. Piszczek, J.R. Lakowicz, " Enhanced Emission Induced by FRET from a Long-Lifetime, Low Quantum Yield Donor to a Long-Wavelength, High Quantum Yield Acceptor," *Journal of Fluorescence*, Vol. 12, Iss. 1 97-103 (2002).
- [11] A. Zastrow, K. Heidler, R. Sah, V. Wittwer, A Goetzberger, "On the conversion of solar radiation with fluorescent planar concentrators," *Photovoltaic Solar Energy Conference*, http://dx.doi.org/10.1007/978-94-009-8423-3_60 (1981).
- [12] *Solar Photovoltaics: Status, Costs, and Trends*. EPRI, Palo Alto, CA: 2009, 1015804.

- [13] S. Woei Leow, C. Corrado, M. Osborn, M. Isaacson, G. Alers, S.A. Carter, "Analyzing luminescent solar concentrators with front-facing photovoltaic cells using weighted Monte Carlo ray tracing," J. Appl. Phys Vol. 113, Issue 21 (2013).
- [14] D. Avnir, D. Levy, R. Reisfeld, "The nature of the silica cage as reflected by spectral changes and enhanced photostability of trapped Rhodamine-6G," J. Phys. Chem. 88, 5956-5959 (1984).
- [15] V. Sholin, J.D. Olson, S.A. Carter, "Semiconducting polymers and quantum dots in luminescent solar concentrators for solar energy harvesting," J. Appl. Phys. 101, 123114 (2007).
- [16] M.G. Hyldahl, S.T. Bailey, B.P. Wittmershaus, "Photo-stability and performance of CdSe/ZnS quantum dots in luminescent solar concentrators," Solar Energy, Vol. 83, Issue 4, 566-573 (Apr 2009).
- [17] M.J. Currie, J.K. Mapel, T.D. Heidel, S. Goffri, M.A. Baldo, "High-efficiency organic solar concentrators for photovoltaics," Science 321 (5886), 226-228 (2008).
- [18] C. Mulder, P. Reuswig, A. Velázquez, H. Kim, C. Rotschild, M. Baldo, "Dye alignment in luminescent solar concentrators: I. Vertical alignment for improved waveguide coupling," Opt. Express 18, A79-A90 (2010).
- [19] C. Mulder, P. Reuswig, A. Velázquez, H. Kim, C. Rotschild, M. Baldo, "Dye alignment in luminescent solar concentrators: II. Horizontal alignment for energy harvesting in linear polarizers," Opt. Express 18, A91-A99 (2010).
- [20] B.A Swartz, T. Cole, A.H. Zewail, "Photon trapping and energy transfer in multiple-dye plastic matrices: an efficient solar-energy concentrator," Optics Letters Vol. 1, No. 2, 73-75 (1977).
- [21] S.T. Bailey, G.E.Lokey, M.S. Hanes, J. Shearer, J.B. McLafferty, G.T. Beaumont, T.T. Baseler, J.M Layhue, D.R. Broussard, Y. Zhang, B.P. Wittmershaus, "Optimized excitation energy transfer in a three-dye luminescent solar concentrator," Sol. Energy Mat. Vol. 91, 67-75 (2007).
- [22] T. Förster, "Zwischenmolekulare Energiewanderung und Fluoreszenz," Annalen der Physik Vol 437: 55–75(1948).
- [23] J.R. Lakowicz. Principles of Fluorescence Spectroscopy, Third Edition. Spring Science+Business Media, 2006.

- [24] A. Yekta, J. Duhamel, M.A. Winnik "Dipole-dipole electronic energy transfer. Fluorescence decay functions for arbitrary distributions of donors and acceptors: systems with planar geometry," Chem. Phys. Lett. Vol. 235, 119-125 (1995).
- [25] O.J. Rolinski, D. Birch, "Determination of acceptor distribution from fluorescence resonance energy transfer: Theory and simulation," J. Chem. Phys Vol. 112, No. 20, 8923-8933 (2000).
- [26] J. Sansregret, J.M. Drake, W.R.L. Thomas, M.L. Lesiecki, "Light transport in planar luminescent solar concentrators: the role of DCM self-absorption," Applied Optics, Vol. 22, No. 4, 573-577 (1983).
- [27] L.R. Wilson, B.C. Rowan, N. Robertson, O. Moudam, A.C. Jones, B.S. Richards, "Characterization and reduction of reabsorption losses in luminescent solar concentrators," Applied Optics, Vol. 49, No. 9, 1651-1661 (2010).
- [28] J.S. Batchelder, A.H. Zewail, T. Cole, "Luminescent solar concentrators. 2: Experimental and theoretical analysis of their possible efficiencies," Applied Optics, Vol. 20, Issue 21, p3733-3754 (1981).
- [29] L.G. Brooker, G.H. Keyes, R.H. Sprague, R.H. VanDyke, E. VanLare, G. VanZandt, F.L. White "Studies in the Cyanine Dye Series. XI. The Merocyanines," J. Am. Chem. Soc. Vol. 73. Issue 11, 5326-5332 (1951).
- [30] J.M. Drake, M.L. Lesiecki, D.M. Camaioni, "Photophysics and cis-trans isomerization of DCM," Chemical Physics Letters, Vol. 113, Issue 6, 530-534 (1985).
- [31] S.L. Bondarev, V.N. Knyukshto, V.I. Stepuro, A.P. Stupak, A.A. Turban, "Fluorescence and electronic structure of the laser dye DCM in solutions and in polymethylmethacrylate," Journal of Applied Spectroscopy, Vol. 71, No. 2, 194-201 (2004).
- [32] W. Herbst, K. Hunger, *Industrial Organic Pigments*, 2nd Ed, Weinheim 1997.
- [33] T. Förster, "Transfer Mechanisms of Electronic Excitation," Discuss. Faraday Soc., 27, 7-17 (1959).
- [34] G. Cario, J. Franck "Über sensibilisierte Fluoreszenz von Gasen," Zeitschrift für Physik, Vol. 17, Issue 1, 202-212 (1923).
- [35] W. Grotrian, "Die Absorptionsspektren von Thallium und Indiumdampf," Zeitschrift für Physik Vol. 12, 218-231 (1922).

- [36] O. Klein, S. Rosseland, "Über Zusammenstöße zwischen Atomen und freien Elektronen," Zeitschrift für Physik Vol. 4 Issue 1, 46-51 (1921).
- [37] J. Franck, G. Hertz, "Über Zusammenstöße zwischen Elektronen und Molekülen des Quecksilberdampfes und die Ionisierungsspannung desselben," Verh. Dtsch. Phys. Volume 16, 457–467 (1914).
- [38] J. Franck, "Einige aus der Theorie von Klein und Rosseland zu ziehende Folgerungen über Fluoreszenz, photochemische Prozesse und die Elektronenemission glühender Körper," Zeitschrift für Physik, Vol. 9, Iss. 1, 259-266 (1922).
- [39] O. Oldenberg, "Resonance in Collision Processes," Physical Review, Vol. 87 Num. 5 786-789 (1952).
- [40] J. Franck, P. Jordan, "Anregung von Quantensprüngen durch Stöße," Springer, Berlin, 1926.
- [41] H. Beutler, B. Josephy, "Resonanz bei Stößen zweiter Art," Zeitschrift für Physik, Vol. 58, 581 (1928).
- [42] R.M. Clegg, "The History of FRET," Reviews in Fluorescence Vol. 2006, 1-45 (2006).
- [43] A. Mitchell, M. Zemansky. Resonance Radiation and Excited Atoms. Cambridge University Press, 1934.
- [44] H. Kallmann, F. London, "Über quantenmechanische Energieübertragungen zwischen atomaren Systemen," Zeitschrift für physikalische Chemie. Abteilung B, Vol. 2, Iss. 3, 207-243 (1929).
- [45] L. Nordheim "Zur Theorie der Anregung von Atomen durch Stöße," Zeitschrift für Physik, Vol. 36, 497-539 (1926).
- [46] L. Mensing, "Beitrag zur Theorie der Verbreitung von Spektrallinien," Zeitschrift für Physik, Vol. 34, 611-621 (1925).
- [47] J. Holtsmark "Über die Absorption in Na-Dampf," Zeitschrift für Physik, Vol. 34, 722-729 (1928).
- [48] E. Schrödinger, "Energieaustausch nach der Wellenmechanik," Annalen der Physik, Vol. 83, Iss. 15, 956-968 (1927).

- [49] F. Perrin, " Theorie quantique des transferts d'activation entre molecules de meme espece. Cas des solutions fluorescentes," *Ann. Chim. Phys (Paris)*, Vol. 17, 283-314 (1932).
- [50] J. Perrin, "La fluorescence," *Ann Phys (Paris)*, Vol. 10, 133-159, (1918).
- [51] M.N. Berberan-Santos, "Pioneering Contributions of Jean and Francis Perrin to Molecular Luminescence." *New Trends in Fluorescence Spectroscopy: Applications to Chemical and Life Sciences*. Eds. B. Valeur, J.C. Brochon. Berlin: Springer-Verlag, 2001.
- [52] J. Perrin " Fluorescence et induction moleculaire par resonance," *Comptes rendus hebdomadaires des séances de l'Académie des sciences*, Vol. 184, 1097-1100, (1927).
- [53] J. Perrin, N. Choucroun "Fluorescence sensibilisée en milieu liquide (transfert d'activation par induction moléculaire)," *Comptes Rendus* Vol. 189, 1213-1216 (1929).
- [54] F. London, "Zur Theorie und Systemmatik der Molekularkräfte," *Zeitschrift für Physik*, Vol. 63, 245-249.
- [55] R.S. Knox, "Förster's resonance excitation transfer theory: not just a formula," *Journal of Biomedical Optics*, Vol. 17 Issue 1 (2012).
- [56] P. Feofilov, B. Sveshnikov, "Concentrational depolarisation of the fluorescence of dye solutions," *J. Phys. USSR*, Vol. 3, 493-505 (1940).
- [57] F. Weigert, G. Käppler, "Polarisierte Fluoreszenz in Farbstofflösungen," *Zeitschrift für Physik*, Vol. 25, 99-117 (1924).
- [58] E. Gaviola, P. Pringsheim, "Über den Einfluß der Konzentration auf die Polarisation der Fluoreszenz von Farbstofflösungen," *Zeitschrift für Physik*, Vol. 24, 24-36 (1924).
- [59] P. Dirac, "The Quantum Theory of the Emission and Absorption of Radiation," *Proc. Roy. Soc.* Vol. A114, 243-268 (1927).
- [60] E. Fermi. *Nuclear Physics*. University of Chicago Press, 1950.
- [61] D. Valeur, M. Berberan-Santos, *Molecular Fluorescence: Principles and Applications*, Second Edition. Wiley-VCH Verlag GmbH & Co. KGaA (2012).

- [62] K.T. McDonald, Radiation in the Near Zone of a Hertzian Dipole (April 22, 2004), <http://www.hep.princeton.edu/~mcdonald/examples/nearzone.pdf>
- [63] L. Novotny, B. Hecht. *Principles of Nano-Optics*. Cambridge University Press: Cambridge, 2006.
- [64] M. Patel, M. Bowditch, B. Jones, D. Netherton, N. Khan, S. Letant, R. Maxwell, S. Birdsell, "Volatile out gassing characteristics of highly filled ethylene vinyl acetate binder materials: Gas phase infra-red spectroscopy," *Polymer Testing*, Vol. 32, Iss. 2 313-320 (2013).
- [65] L.R. Wilson, B.S. Richards, "Measurement method for photoluminescent quantum yields of fluorescent organic dyes in polymethyl methacrylate for luminescent solar concentrators." *Applied optics*, 48(2), 212-220 (2009).
- [66] D.L. Dexter "A Theory of Sensitized Luminescence in Solids," *Journal of Chemical Physics*, Vol. 21, No. 5, 836-850 (1953).
- [67] I.Z. Steinberg, "Long-range nonradiative transfer of electronic excitation energy in proteins and polypeptides," *Annual Review of Biochemistry*, Vol. 40: 83 -114 (1971).
- [68] L. Stryer, R.P. Haugland, "Energy transfer: A spectroscopic ruler," *Proc. Natl. Acad. Sci.* 58, 719-726 (1967).
- [69] G. Gabor, "Radiationless energy transfer through a polypeptide chain," *Biopolymers* 6, 809-816 (1968).
- [70] C.A. Parker, W.T. Rees, "Fluorescence spectrometry - a review," *Analyst* Vol. 87, Issue 1031, 83-111 (1962).
- [71] M. Kubista, R. Sjöback, S. Eriksson, B. Albinsson, "Experimental Correction for the Inner-filter Effect in Fluorescence Spectra," *Analyst*, Vol. 119, 417-419 (1994).
- [72] J.C. Boyer, F van Veggel, "Absolute quantum yield measurements of colloidal NaYF₄: Er³⁺, Yb³⁺ upconverting nanoparticles," *Nanoscale*, Vol. 2, Iss. 8, 1417-1419 (2010).
- [73] R.W.G. Hunt, *Measuring Colour*, Wiley, Hoboken USA 2011.
- [74] Schanda, J. *Colorimetry: understanding the CIE system*. Wiley-Interscience, Hoboken, USA 2007.